2021-06-21

Ubiquitin Signaling Regulates P-Body Assembly

Kedia, Shreeya

UNIVERSITY OF CALGARY

Ubiquitin Signaling Regulates P-Body Assembly

by

Shreeya Kedia

A THESIS

SUBMITTED TO THE FACULTY OF GRADUATE STUDIES

IN PARTIAL FULFILMENT OF THE REQUIREMENTS FOR THE

DEGREE OF MASTER OF SCIENCE

GRADUATE PROGRAM IN BIOCHEMISTRY AND MOLECULAR BIOLOGY

CALGARY, ALBERTA

JUNE, 2021

Abstract

During the development of the central nervous system, neural stem cells give rise to different cell populations including neurons and glia. To ensure the genesis of the correct cell populations in the developing brain, there exists and intricate system of gene expression regulation. One such mechanism of gene expression regulation is the presence of membrane-less ribonucleoprotein (RNP) granules in the cell such as Processing bodies (PBs). These dynamic organelles are sites of RNA metabolism that can temporarily sequester mRNAs resulting in translational repression and/or decay. Therefore, to understand the molecular mechanism by which PBs regulate stem cell homeostasis, it is critical to delineate the signaling regulating PB dynamics. To this end, my thesis explores a novel non-proteolytic monoubiquitination-based signaling mechanism, where monoubiquitination of a core PB protein called 4E-T drives PB assembly. Mechanistically, PB dynamics are fine-tuned by a deubiquitinase called Otud4, which deubiquitinates 4E-T to disassemble PBs. This dynamic ubiquitination signaling therefore, functions as an essential molecular switch to coordinate PB dynamics in neural stem cells.

Acknowledgement

I am grateful to Dr. Guang Yang for his guidance and encouragement throughout my MSc. Thank you for providing this opportunity. I would like to thank my supervisory committee members Dr. Peng Huang and Dr. Paul Mains for their guidance and helpful insights into my research. I would like to acknowledge Mitacs Globalink Graduate Fellowship and Alberta Children's Hospital Research Institute Graduate Scholarship for funding me during the duration of my Masters.

I would like to thank all members of the Yang Laboratory for their useful research insights and support. For that I thank Brooke Rackel, Laura Williams, Mohammadreza Aghanoori, Rejitha Suraj, Lamees Mohammed, Emily Harvey, Drayden Kopp and Xin Chen. I would particularly like to thank our lab technician, Sarah Erickson for all her help with the mouse work as well as with invitro neural stem cell cultures. I would additionally like to thank Kaylan Burns and Pengqiang Wen for all their help with cloning as well as everybody associated with the project.

Lastly, I would like to thank all my friends and family, especially my parents and my sister for their unconditional support always.

Table of Contents

List of Figures and Tables

Figures

Tables

List of Abbreviations

Symbol/Abbreviation	Definition
Eif4enif1 (4E-T)	Eukaryotic translation initiation factor 4E transporter
ALS	Amyotrophic Lateral Sclerosis
ASD	Autism Spectrum Disorder
ATP	Adenosine triphosphate
bHLH	Basic Helix-Loop-Helix
Cnot7	CCR4-NOT transcription complex subunit 7
CNS	Central Nervous System
CP	Cortical Plate
Cpeb3	Cytoplasmic polyadenylation element-binding protein 3
Csde1	Cold shock domain containing protein E1
Dcaf7	DDB1-and CUL4- associated factor 7
Dcp1a	mRNA decapping enzyme subunit 1a
Dcp2	mRNA decapping enzyme subunit 2
Ddx3X	DEAD-box helicase 3 X-Linked
Ddx6	Dead box helicase 6
DMEM	Dulbecco's Modified Eagle Medium
DMSO	Dimethyl Sulfoxide
DTT	Dithiothreitol
DUB	Deubiquitinase
ECL	Enhanced chemiluminescence
Edc3	Enhancer of mRNA decapping protein 3
Edc4	Enhancer of mRNA decapping protein 4
EDTA	Ethylenediaminetetraacetic acid
Eif4e2	Eukaryotic translation factor 4E family member 2
FBS	Fetal Bovine Serum
FGF2	Fibroblast Growth Factor 2
FTD	Frontotemporal Dementia

G3bp	Ras-GAP SH3 domain binding protein
GFP	Green Fluorescent Protein
HBSS	Hank's Balanced Salt Solution
HEK293	Human Embryonic Kidney 293 cells
HRP	Horseradish Peroxidase
Igf2bp1	Insulin-like growth factor 2 mRNAbinding protein 1
IPs	Intermediate Progenitors
LLPS	Liquid-Liquid Phase Separation
MEM	Minimal Essential Medium
miRISC	Micro-RNA induced silencing complex
NDS	Normal Donkey Serum
NSC	Neural Stem Cell
oRG	Outer Radial Glia
Otud4	Ovarian tumor domain containing protein 4
PAGE	Polyacrylamide gel electrophoresis
Pax6	Paired box 6
PB	Processing Body
PBS	Phosphate-buffered saline
PEI	Polyethylenimine
PFA	Paraformaldehyde
PMSF	Phenylmethylsulfonyl fluoride
Pum2	Pumilio2
Rc3h1	Roquin-1
RG	Radial Glia
Rnf214	RING finger protein 214
RNP	Ribonucleoprotein
SDS	Sodium dodecyl sulfate
SG	Stress Granule
Stau2	Staufen2
SVZ	Subventricular Zone
TBS-T	Tris Buffered Saline (with Tween20)

Tdp43	TAR DNA-binding protein 43
Top3b	DNA topoisomerase 3-beta-1
Trim56	Tripartite motif containing protein 56
VZ	Ventricular Zone

Chapter 1

Introduction

1.1 Overview

The development of complex organ systems such as the mammalian brain relies on the ability of stem cells to undergo self-renewal while giving rise to different cell types (Hall and Watt, 1989). For instance, during development, neural stem cells (NSCs) in the brain are capable of self-renewal as well as differentiation into different cell types including neurons and glia (Götz and Huttner, 2005). To ensure proper development, there exists a delicate balance between this self-renewal and differentiation regulated by precise gene expression. Central to this precision is cellular compartmentalization facilitated by membrane-bound and membrane-less organelles, which allows spatial regulation of different steps of gene expression. Previous research has explored the role of membrane-bound organelles (such as mitochondria, endoplasmic reticulum, Golgi bodies) in regulating neural stem cell fate decision (Iwata et al., 2020; Khacho et al., 2016; Wu et al., 2016; Xie et al., 2018). However, the role of membrane-less organelles (such as P-bodies, stress granules amongst others) in regulating neural stem cell fate is not well characterized.

Recent evidence suggests one such membrane-less organelle called Processing Bodies (PBs) are critical regulators of stem cell fate (Yang et al., 2014). These PBs are cytoplasmic ribonucleoprotein (RNP) granules that regulate RNA metabolism in the cell by sequestering mRNAs away from the translation machinery preventing their translation. To understand how PB dynamics can regulate neural stem cell homeostasis, it is critical to first delineate molecular signaling mechanism regulating PB assembly/disassembly. Therefore, my project focuses on characterizing a non-proteolytic ubiquitination-based signaling mechanism regulating PB

dynamics. I hypothesize that reversible monoubiquitination of 4E-T, a critical component of PBs triggers PB assembly.

1.2 Specific Aims:

Aim 1: To assess the ubiquitination of 4E-T and its correlation with PB assembly.

Previous research hinted at ubiquitination being a possible signaling mechanism regulating PB dynamics (Tenekeci et al., 2016; Ukmar-Godec et al., 2019). In this chapter, the role of ubiquitination on PB dynamics was first analysed using a ubiquitination inhibiting drug. Next, ubiquitination of core PB proteins was assessed and analysed using immunoprecipitation and SDS-PAGE. I found that 4E-T, a core PB component was monoubiquitinated. Since monoubiquitination often serves signaling functions in the cell, the remainder of the study focused on assessing the role of 4E-T ubiquitination on PB assembly. Further, in this chapter, using various experiments, monoubiquitination of 4E-T was confirmed and correlation between PB dynamics and 4E-T monoubiquitination was assessed.

Aim 2: To examine the molecular process monoubiquitination of 4E-T regulates PB assembly

This chapter asked if the lack of ubiquitination prevents the targeting of 4E-T to PBs and additionally, its impact on endogenous PB formation. RNP granules such as PBs assemble through sequential RNA-protein interactions (Hubstenberger et al., 2017). To understand the biochemical mechanism of 4E-T ubiquitination-mediated PB assembly, this chapter assessed how 4E-T ubiquitination alters 4E-T interaction networks to regulate PB formation.

Aim 3: To determine how the deubiquitinase Otud4 regulates the dynamic monoubiquitination of 4E-T and P-body assembly

Monubiquitination is reversible and is dynamically regulated by enzymes called E3 ligases and deubiquitinases. The aim of this chapter was to first identify the deubiquitinase regulating 4E-T and further to assess the role of this deubiquitinase in regulating PB dynamics.

1.3 Significance:

The aim of this thesis was to delineate a ubiquitination-based signaling mechanism regulating PB dynamics. While previous research hinted at ubiquitination as a possible regulator for PB dynamics, the exact molecular targets and pathway still remains unknown (Tenekeci et al., 2016; Ukmar-Godec et al., 2019). Additionally, how this ubiquitination/deubiquitination cycle can regulate neural stem cell fate is poorly understood. Broadly, understanding this 4E-T monoubiquitination mediated signaling will not only help understand PB dynamics, but will also provide a useful tool to address the effects of PB dynamics on neural stem cell homeostasis.

Chapter 2

Literature Review

2.1 Development of the embryonic cortex

Early in mammalian brain development, the telencephalic wall is lined by a single sheet of undifferentiated neuroepithelial cells which proliferate and expand in number. With the switch to neurogenesis, some of the neuroepithelial cells differentiate and give rise to neural progenitor cells called radial glia. During the development of the Central Nervous System (CNS), these radial glial cells line the ventricular zone (VZ) and constitute the primary neural progenitor cell type giving rise to the majority of neurons throughout the CNS **(Figure 1)**. These RG cells additionally differentiate and give rise to other progenitor classes like outer radial glia (oRGs) and intermediate progenitors (IPs), establishing the subventricular zone (SVZ) (Götz and Huttner, 2005; Kriegstein and Alvarez-Buylla, 2009). In mice, these neural progenitor populations begin differentiating into neurons around embryonic day 10.5 (E10.5). Using radial glial cells as a scaffold, the new-born neurons migrate away from the ventricular zone and populate the cortical plate (CP) (Noctor et al., 2001). The cortical plate consists of six defined layers arranged in an inside-out organization, with early born neurons populating deeper cortical layers such as layer VI/V and later born neurons giving rise to more superficial layers such as layer IV/III/II (Custo Greig et al., 2013a).

To ensure proper brain development, it is critical to maintain a steady stem cell pool as neural precursor cells first differentiate into neurons and after termination of neurogenesis, adopt a gliogenic phase, giving rise to astrocytes and oligodendrocytes. Therefore, to prevent premature exhaustion of the neural stem cell pool, neural stem cells can either undergo symmetric divisions generating two daughter cells of the same fate or asymmetric division, giving rise to a neural stem cell and a neuron. This delicate balance between symmetric and

asymmetric division is orchestrated by a sophisticated mechanism of gene expression regulation (Martynoga et al., 2012). Errors in this process have been implicated in neurodevelopmental disorders such as Autism Spectrum Disorder (ASD) and schizophrenia (Durak et al., 2016; Gkogkas et al., 2013; Kim et al., 2012; Orosco et al., 2014).

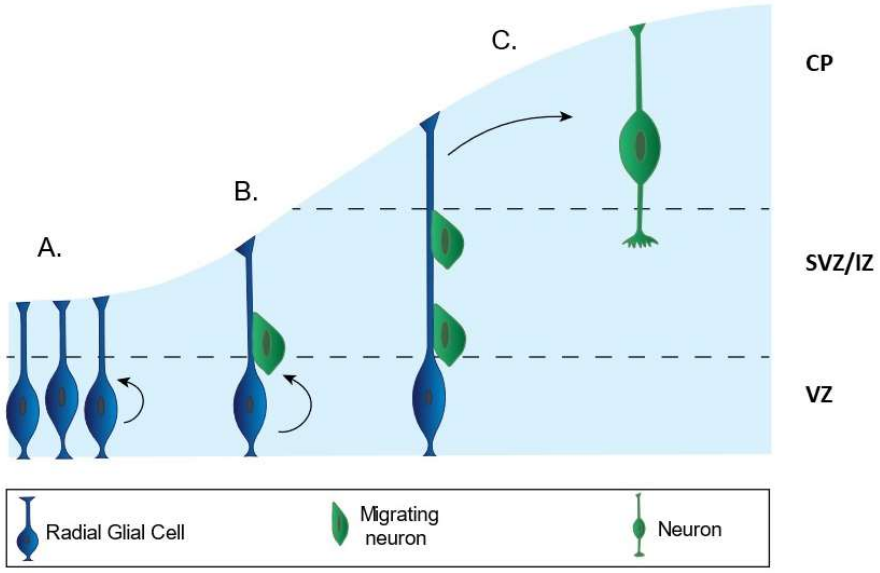

Figure 1. Cortical neurogenesis in the developing embryonic mouse cortex. (A) Early in development radial glial (RG) cells proliferate and expand the neural progenitor pool in the ventricular zone (VZ) (Custo Greig et al., 2013b). (B-C) At embryonic day 11.5 (E11.5), these RG cells begin to differentiate into neurons, which further migrate up using RG cells as a scaffold, establishing the cortical plate (CP) (Imayoshi and Kageyama, 2014). The CP consists of six layers and is established in an inside-out pattern, where deeper cortical layers (layer VI/V) are populated first, followed by more superficial layers (layer IV/III/II) (Custo Greig et al., 2013b).

2.2 Coordinated gene expression regulates stem cell homeostasis

To ensure proper cortical development, gene expression is regulated at multiple levels, including transcriptional, posttranscriptional, translational and post-translational levels of regulation. The transcriptional programs that instruct stem cell homeostasis have been extensively studied. Previous research has implicated the role of basic helix-loop-helix (bHLH) transcriptional factors in regulating neural stem cell proliferation and neurogenesis as well as for generation of glia like astrocytes and oligodendrocytes (Imayoshi and Kageyama, 2014; Muroyama et al., 2005). Additionally, during cortical development, transcription factors such as Paired box 6 (Pax6) are crucial regulators of the neurogenic potential of neural stem cells (Heins et al., 2002).

Recent studies have also delineated post-transcriptional/translational level programs regulating neural stem cell fate. For instance, RNA-binding proteins such as Staufen2 (Stau2) and Pumilio2 (Pum2) asymmetrically localize to neural stem cells and prevent their premature differentiation by binding to and repressing translation of pro-neurogenic mRNAs (Vessey et al., 2012; Zhang et al., 2017). Additionally, methylglyoxal, a glycolytic intermediate metabolite, supresses translation of *Notch1* mRNA, inducing neural stem cell differentiation into neurons (Rodrigues et al., 2020).

Besides transcriptional and translational level programs, recent research has also identified the role of post-translational modifications in modulating neural stem cell fate decisions. For instance, Tripartite motif containing 32 (Trim32), an E3 ubiquitin ligase and Ubiquitin specific protease 7 (Usp7), a deubiquitinase counter regulate degradation of c-Myc, a transcription factor critical for neural stem cell maintenance (Nicklas et al., 2019). Trim32 localizes asymmetrically to neural stem cells and promote their differentiation to neurons (Schwamborn et al., 2009). On the other hand, E3 ubiquitin ligase Tripartite containing motif

11 (Trim11), ubiquitinates and degrades transcriptional factor Pax6, promoting neural stem cell fate maintenance (Tuoc and Stoykova, 2008).

This multi-level regulation of gene expression, therefore, is critical to regulate stem cell homeostasis and to ensure the genesis of the correct number and type of neurons.

2.3 Cellular compartmentalization in eukaryotic cells

Previous research has delineated that multi-level regulation of gene expression is critical for the increased functional complexity of eukaryotic cells. This is achieved by the presence of an intricate system of cellular compartmentalization through spatial organization of its functional components, facilitated by the presence of membrane-bound and membrane-less organelles in the cell (Diekmann and Pereira-Leal, 2012; Gabaldón and Pittis, 2015; Mason et al., 2019). Membrane-bound organelles (such as nucleus, mitochondria, Golgi bodies, endoplasmic reticulum, amongst others) are hallmarks of cellular compartmentalization and provide critical spatiotemporal control in a wide range of biological applications such as gene expression regulation. For instance, in eukaryotes, the nucleus sequesters the transcription machinery away from the translation machinery, allowing more sophisticated regulation of gene expression by post-transcriptional modifications (Boeynaems et al., 2018).

Living cells also contain dynamic organelles, lacking a defining membrane, such as P-bodies, P-granules, stress granules, Cajal bodies, paraspeckles, amongst others, that can assemble and disassemble within the aqueous environment (Hyman et al., 2014) **(Figure 2)**. These condensates have been implicated in wide range of biological applications including mRNA metabolism, gene expression regulation, DNA damage repair, amongst others (Hyman et al., 2014; Mitrea et al., 2018; Oshidari et al., 2020). These membrane-less organelles often co-exist as liquid drops in the cytoplasm and/or nucleus and their formation is regulated by

liquid-liquid phase separation (LLPS), wherein these macromolecules simultaneously assemble into a dense and dilute phase (Alberti et al., 2019). LLPS is energetically favourable and is dependent on physiological conditions like temperature, pH, salt concentration, amongst others. LLPS is often mediate by a class of macromolecules called scaffold proteins, that drive this liquid-liquid de-mixing. In addition, these condensates also contain another class of macromolecules called clients, which often bind to scaffold proteins to phase separate into these condensates.

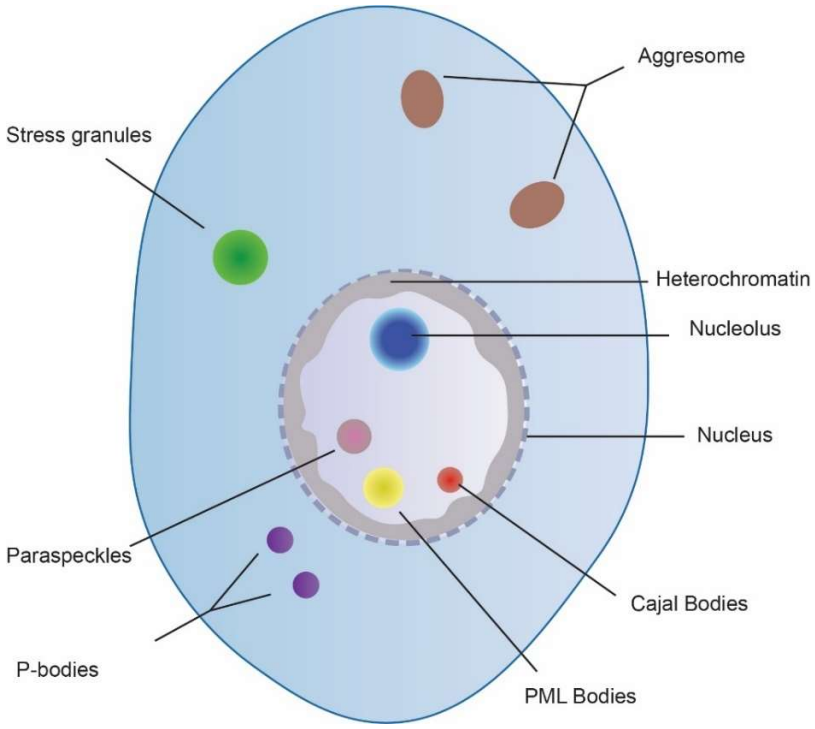

Figure 2. Membrane-less organelles facilitate cellular compartmentalization. Liquid-liquid phase separation mediates assembly of a wide range of membrane less organelles within the cell. The figure depicts some of the membrane-less organelles commonly found in eukaryotic cells. (Adapted from Gomes and Shorter, 2019; Sanders et al., 2020).

This dynamic compartmentalization offers several advantages: First, LLPS allows the cells to fine-tune their biochemical environment by concentrating macromolecules at a single site, affecting reaction kinetics. Second, the dynamic assembly and disassembly offer a faster, reversible, and tuneable switch allowing cells to adapt rapidly to the changing environmental cues. Third, sequestering of macromolecules into these liquid-liquid phase separated condensates can additionally alter their localization, affecting their biochemical function (Alberti et al., 2019). For instance, P-bodies (PBs), a type of RNA-protein (RNP) granule in the cytoplasm temporarily sequesters specific mRNAs, preventing their translation (Brengues et al., 2005).

Cellular compartmentalization in eukaryotic cells allows formation of complex organ systems such as the mammalian brain. The role of membrane-bound organelles in stem cell homeostasis has been extensively studied (Iwata et al., 2020; Khacho et al., 2016; Wu et al., 2016; Xie et al., 2018). However, how membrane-less organelles regulate neural stem cell fate still remains poorly characterized.

Recent research has explored how dysregulation of these membrane-less RNP granules could result in neurodevelopmental disorders. For instance, a recent study discovered that *de novo* germline mutations in DEAD-box helicase 3 X-Linked (DDX3X), an RNA helicase localised in stress granules, affect RNA metabolism impairing neurogenesis. This mutation has been associated with a rare neurodevelopmental disorder resulting in cortical malformation, epilepsy and autism in affected individuals (Lennox et al., 2020). Additionally, another RNA-binding protein family called ELAV-like (Elavl), predominantly present in RNA transport granules have been associated with epilepsy, intellectual disability, and autism (Fernandopulle et al., 2021; Popovitchenko et al., 2020), suggesting that these RNP granules are critical regulators of neurogenesis.

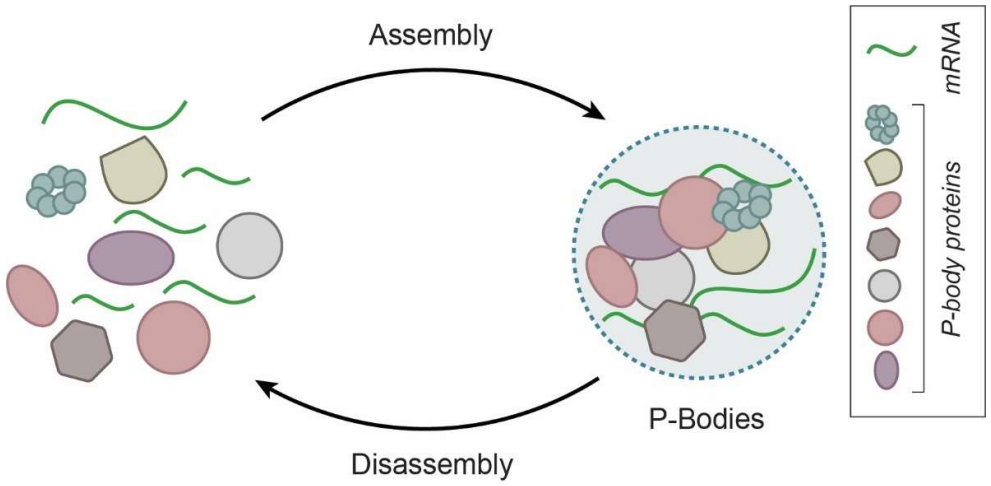

Figure 3. Multivalent interactions promote PB assembly. Schematic depicting multivalent interactions between core PB proteins such as 4E-T, Ddx6, Cnot7, Lsm1-7, Lsm14A, Dcp1/2 and Edc3/4.

2.4 Role of P-bodies in cortical development

One such membrane-less organelle conserved across all eukaryotic organisms are cytoplasmic RNP granules present in the cytoplasm called P-bodies (Eulalio et al., 2007a) and these will be a focus of my thesis. PBs assemble through sequential multivalent RNA-protein interactions, wherein a small group of proteins serve as the scaffold, followed by recruitment of additional client proteins for maturation (Banani et al., 2016; Guillén-Boixet et al., 2020; Van Treeck and Parker, 2018) **(Figure 3)**. PBs regulate gene expression through context-dependent mRNA translation repression and/or decay (Luo et al., 2018; Wang et al., 2018). At the molecular level, PBs constitute repressed mRNAs, micro-RNA mediated silencing complex (miRISC), decapping complexes and 5' to 3' exonucleases (Hubstenberger et al., 2017). Previous research has delineated that depending on the mRNA and/or context, PBs can either target mRNAs for decay or alternatively temporarily store mRNAs by sequestering them away

from translation machinery. This translation repression is reversible and mRNAs can later return to cytosol to re-enter translation (Brengues et al., 2005) **(Figure 4)**.

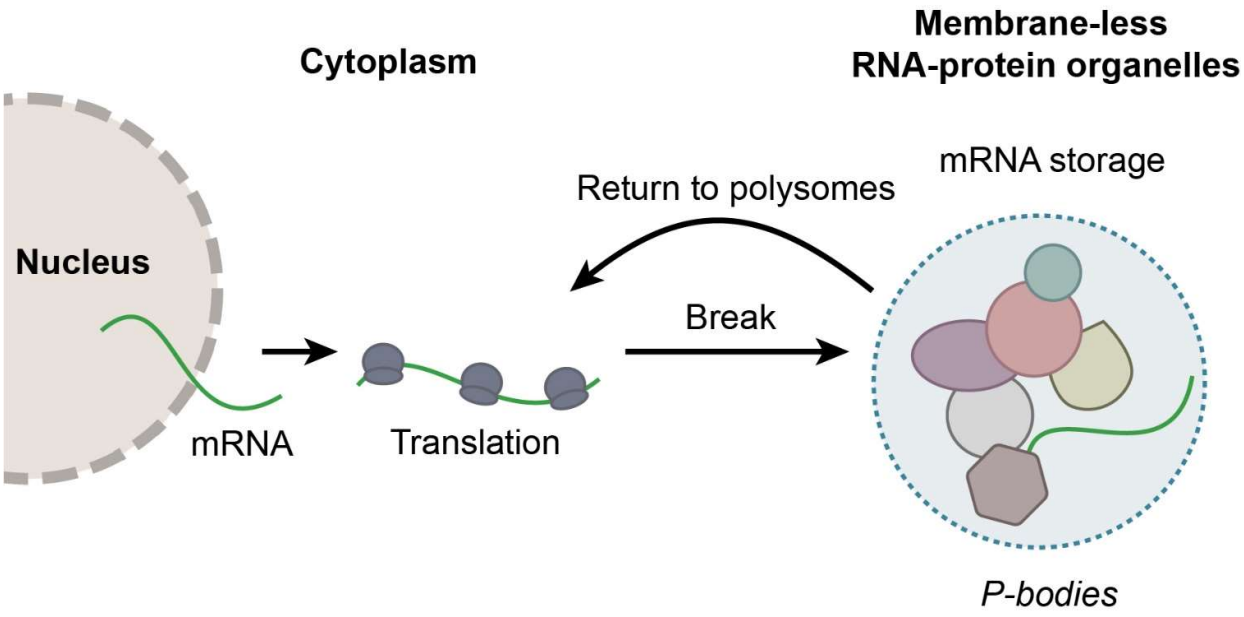

Figure 4. PBs mediate reversible translational repression. PBs can temporarily sequester mRNAs away from translational machinery suppressing their translation. On dissolution of PBs, mRNAs can return to polysomes for translation.

Previous studies have hinted that PBs are critical for regulating proper cortical development. During neurogenesis, 4E-T, a critical component of PBs, selectively bind pro-differentiation mRNAs, repressing their translation and facilitating neural stem cell fate maintenance. Post-translational regulation of 4E-T is a major topic of this thesis. Disruption in this process results in premature differentiation of neural stem cells into neurons, prematurely exhausting the neural stem cell pool (Yang et al., 2014) **(Figure 5).**

A.

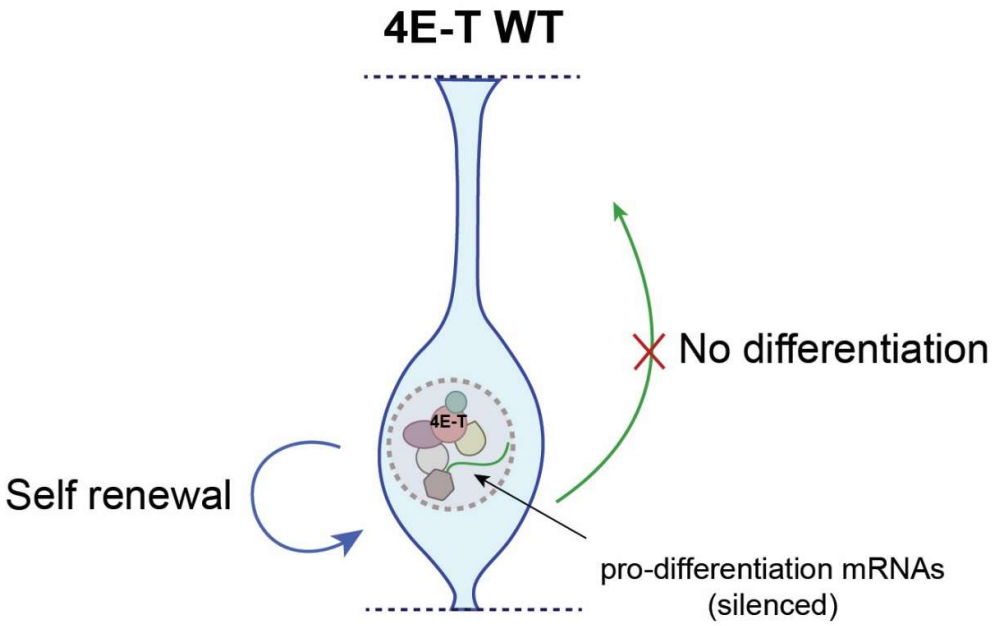
4E-T WT
No differentiation
4E-T
Self renewal
pro-differentiation mRNAs
(silenced)

B.

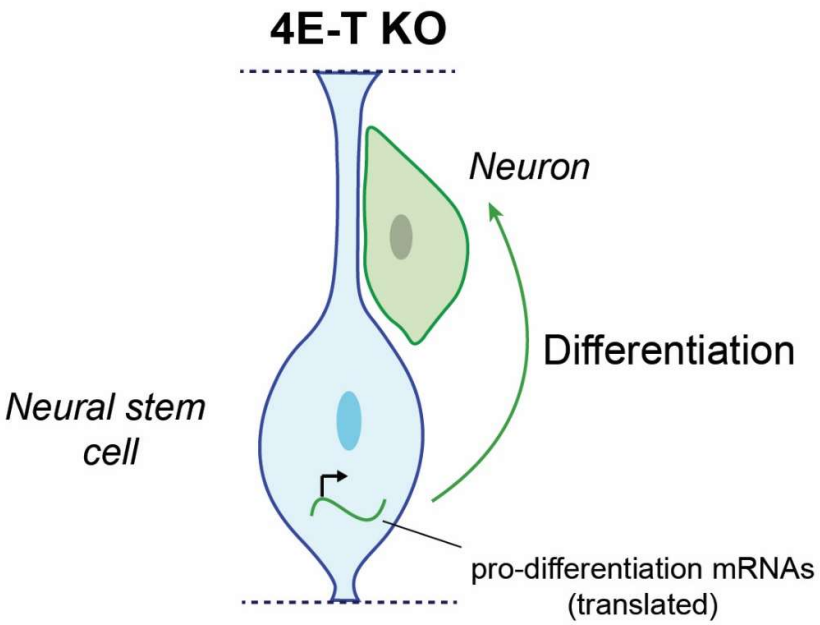
4E-T KO
Neuron
Differentiation
Neural stem
cell
pro-differentiation mRNAs
(translated)

Figure 5. 4E-T regulates cortical neurogenesis. Neural precursor cells are transcriptionally primed to generate neurons. (A) In neural stem cells, 4E-T, a core PB protein, promotes stem cell renewal by sequestering pro-differentiation mRNAs in PBs and suppressing their translation (Yang et al., 2014). This allows neural stem cells to proliferate and expand in number, establishing a neural stem cell pool. (B) Loss of 4E-T results in the translation of pro-differentiation mRNAs, resulting in the premature differentiation of neural stem cells into neurons (Yang et al., 2014).

Furthermore, during mammalian brain development, neural stem cells can give rise to different neuronal subtypes, which arrange themselves into different neocortical layers. Deep layer neurons are generated first and populate deeper cortical layers, whereas more superficial layer neurons are generated later giving rise to upper cortical layers. The 4E-T complex has been implicated to selectively repress translation of a subset of neuronal identity mRNAs, allowing temporal control of neuronal subtype specification (Zahr et al., 2018). While all evidence suggests PBs are critical regulators of proper mammalian brain development, the exact molecular mechanism regulating PB dynamics remains largely unknown.

2.5 Post-translational modifications regulating PB dynamics

PBs are highly dynamic and to understand their role in neural stem cell homeostasis, it would be critical to first understand the molecular mechanism regulating PB dynamics. Post-translational modifications play a critical role in cell signaling (Deribe et al., 2010). Previous research has shown that in yeast during stress phosphorylation of Dcp2 is required for its targeting to PBs (Yoon et al., 2010). Additionally, it has been shown that K63-linked

ubiquitination of Dcp1a induces its phosphorylation regulating mRNA decapping and decay as well as altering PB remodelling (Tenekeci et al., 2016). Furthermore, a previous study has shown that post-translational modification of cytoplasmic polyadenylation element-binding protein 3 (Cpeb3) by small ubiquitin like modifier (SUMOylation) regulates mRNA translational repression by targeting it to PBs. De-SUMOylation targets Cpeb3 to polysomes promoting mRNA translation (Ford et al., 2019). These findings suggests that post-translational modifications are critical players regulating PB dynamics and function.

2.6 Role of ubiquitination in regulating PB dynamics

Previous research has hinted at the role of covalent modifications such as ubiquitination as a plausible molecular switch regulating PB dynamics. Studies have identified that PB proteins show a higher incidence of lysine residues, allowing post-translational addition of ubiquitin (Ukmar-Godec et al., 2019). Additionally, a general ubiquitin knock-down caused a decrease in PB assembly, indicating that ubiquitination is a critical regulator modulating PB dynamics (Tenekeci et al., 2016).

Protein ubiquitination is a critical post-translational modification regulating cellular function in eukaryotic cells. It is characterized by the addition of a 76-amino acid ubiquitin moiety, covalently attached to the lysine of the substrate (Xu and Jaffrey, 2011). Depending on the number of ubiquitin attached to the substrate, protein ubiquitination can be classified into two categories: First, if only one ubiquitin attaches to the substrate, it is called monoubiquitination and it often signaling functions (Tai and Schuman, 2008). Second, if more than one ubiquitin attaches, it is called polyubiquitination and it often targets protein to the proteasome for degradation (Akutsu et al., 2016; Herhaus and Dikic, 2015) **(Figure 6)**.

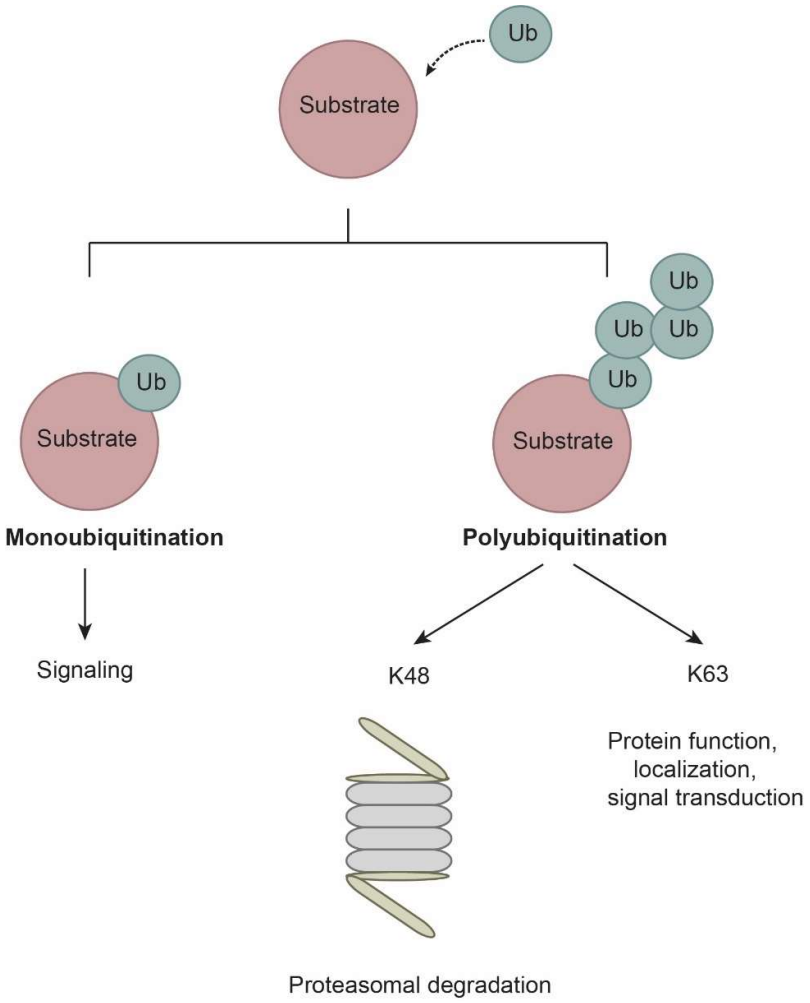

Figure 6. Schematic depicting types of ubiquitination. Single ubiquitin attachment to the substrate is called monoubiquitination and it often serves signaling functions. On the other hand if more than one ubiquitin attaches it is called polyubiquitination. Ubiquitin consists of seven lysines (K6, K11, K27, K29, K33, K48, K63) and one methionine (M1), which facilitate attachment of subsequent ubiquitin moieties to form different polyubiquitin chains. Two of the most studied chains include: K48 polyubiquitin chains, which target substrate for degradation by the proteasome and K63 chains, which are involved in signal transduction as well as affect protein structure and function.

Protein ubiquitination involves a three-step enzymatic cascade, wherein a ubiquitin moiety is first activated in an ATP-dependent manner by a ubiquitin activating enzyme (E1). This activated ubiquitin is then transferred to a ubiquitin conjugating enzyme (E2) forming a E2-Ub intermediate. This intermediate binds to ubiquitin ligase (E3) facilitating transfer of ubiquitin from E2 to the substrate. An interesting feature about ubiquitination is that this process is reversible. Another class of enzymes called deubiquitinases can remove ubiquitin from the target protein and deconstruct the polyubiquitin chains to maintain ubiquitin homeostasis within the cell. This reversible nature of ubiquitination facilitates its function as an ON/OFF switch in regulating cell signaling (Deribe et al., 2010; Herhaus and Dikic, 2015; Tai and Schuman, 2008) **(Figure 2)**.

To understand how PBs regulate proper neocortical development, it would first be critical to delineate the molecular mechanism regulating PB dynamics. To this end, my thesis explores a non-proteolytic ubiquitination-based mechanism driving PB assembly and subsequently its role in neural stem cell homeostasis.

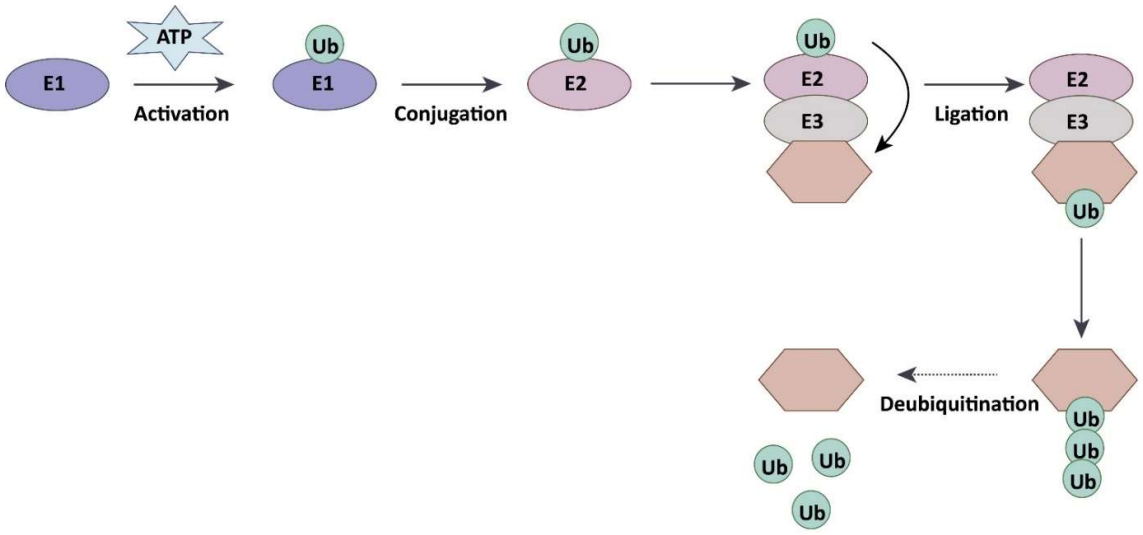

Figure 7. Protein ubiquitination pathway. Ubiquitination involves a three-step enzymatic cascade. Ubiquitin is first activated in an ATP dependent manner by an enzyme called ubiquitin activating enzyme (E1) and transferred to the ubiquitin conjugating enzyme (E2). An enzyme called E3 ligase binds simultaneously to this E2-ubiquitin intermediate and the substrate and transfers ubiquitin to the substrate. This results in ubiquitination of the target protein. Additionally, in the cell ubiquitin proteases called deubiquitinases maintain ubiquitin homeostasis by removing ubiquitin from the target protein.

Chapter 3

Materials and Methods

3.1 Animals: All animal use was approved by the Animal Care Committee at the University of Calgary in accordance with animal use protocol AC17-0099. Female CD1 mice (8–12 weeks old) were used for all animal experiments and were purchased from Charles River Laboratory. Mice were housed in groups of one to five per cage, with a standard 12-hour light-dark cycle in a room maintained at 24°C with free access to water and chow. The morning of vaginal plug detection was designated as embryonic day (E) 0.5.

3.2 Antibodies: For immunoprecipitation, antibodies used included mouse anti-V5 (Thermo Fisher Scientific #R960-25), rabbit anti-GFP (Abcam #ab290) and rabbit anti-DDK (Abcam #ab1162). For immunoblotting, antibodies used included rabbit anti-GFP (1:5000, Abcam #ab290), rabbit anti-DDK (1:5000, Abcam #ab1162), rabbit anti-HA (1:2000, Abcam #ab9110), rabbit anti-MYC (1:2000, Abcam #ab9106) and mouse anti-V5 (1:5000, Thermo Fisher Scientific #R960-25). For immunostaining, antibodies used included rabbit anti-GFP (1:1000, Abcam #ab290), chicken anti-GFP (1:1000, Millipore #AB16901), mouse anti-4E-T (1:100, Abnova #H00056478-B01), mouse anti-DCP1a (1:100, Abnova #H00055802-M06) and rabbit anti-EDC4 (1:500, Cell Signaling #2548).

3.3 Cell culture: HEK293 cells were cultured in Dulbecco's Modified Eagle Media (DMEM) (Gibco #11995-065) supplemented with 10% Fetal Bovine Serum (FBS) (Wisent #098-150) and 1% Pencillin-Streptomycin antibiotic (Wisent #450-201-EL) solution at 37ºC with 5% CO_2.

3.4 Neural stem cell culture: For primary neural precursor cell cultures, pregnant CD1 mice were euthanised using isoflurane and cervical dislocation according to the animal use protocol. CD1 mouse embryos were collected at embryonic day 12.5 (E12.5) and placed in ice-cold Hank's Balanced Salt Solution (HBSS) to retain cell viability. The meninge was removed and the cortex was dissected from each embryonic brain in ice-cold HBSS under the microscope and transferred to Neurobasal media (Gibco #21103-049) supplemented with 2% B-27 (Thermo Fisher Scientific #17504044), 0.5 mM L-Glutamine (Sigma #56-85-9), 1% Penicillin-streptomycin solution (Wisent #450-201-EL) and 40 ng/mL Fibroblast Growth Factor 2 (FGF2) (Thermo Fisher Scientific #CB-40060A). To obtain a single cell suspension tissues were mechanically triturated with a plastic Pasteur pipette and filtered through a 40 µm strainer (VWR #10199-655). Neural stem cells were plated at a density of 250,000 cells/mL on coverslips pre-coated with 5 mg/mL laminin (VWR #CACB354232) and 1 mg/mL poly-D-lysine (VWR #P6407).

3.5 Transfection: For transfection of HEK293 cells at 70-80% confluency, 4.5 million cells were seeded one day prior to transfection. The following day, 5-15 µg DNA was transfected using polyethylenimine (PEI) (Polysciences 29320-38-5) as a transfection agent in the ratio of 1:3 to total DNA added (see Section 3.5.1). This was topped up to 1 mL using opti-MEM (Minimum Essential Media) (Thermofisher Scientific #31985070), mixed thoroughly and incubated at room temperature for 30 minutes. This mixture was then added dropwise to the cells. The cells were incubated at 37ºC followed by change of media three hours after transfection.

NSCs were transfected with 1-2 µg DNA, 4 hours after plating using Lipofectamine Stem transfection agent (Thermofisher Scientific #STEM00008) in the ratio of 1:2 to total

DNA added. This was topped to 50 µL opti-MEM, mixed thoroughly, incubated for 15 minutes at room temperature, and added dropwise to the cells. The cells were analyzed 3 days after transfection.

3.5.1 Preparation of PEI stock solution for transfection: To prepare PEI solution for transfection, 100 mg of PEI powder of PEI powder was dissolved in 100 mL of water and pH was adjusted to 7.0 using HCl. The solution was filtered through 0.22 µm membrane. This not only ensures sterility during cell culture but also helps increase transfection efficiency by filtering out any undissolved particles of PEI, which may precipitate DNA. The PEI solution can be stored in -80ºC or in 4ºC for up to two months.

3.6 Plasmids: The pEF1α-EGFP plasmid expressing nuclear EGFP and DDK- or EGFP-tagged 4E-T plasmids have been previously reported 23. The V5 tag was introduced at the N- or C-terminus of 4E-T by PCR with primers comprising the V5 sequence and subcloned into the pcDNA3 vector. The 4E-T KR mutant was synthesized by Thermo Fisher Scientific and subcloned into pEGFP-C1, pCAGIG or pcDNA3 with indicated tags. To generate Ubi-4E-T, a single copy of the ubiquitin (G76V)-coding sequence from the Ub-G76V-GFP plasmid (Addgene, #11941) was fused to the 4E-T KR-V5 mutant in the pcDNA3 vector by PCR. Mouse Top3b, Dcaf7, Trim56 and Otud4 and human Rc3h1 and Rnf214 were cloned into the pEGFP-C1 vector using cDNA libraries prepared from mouse cortical tissues and HEK293 cells, respectively, with the following primers: Top3b-forward: ATG AAG ACC GTG CTC ATG GTA G-3', Top3b-reverse: 5'-GCA TTT TAA TGG TTT CAG TGG CTC-3'; Dcaf7-forward: 5'-ATG AAC TCC AAA GTC TCC TCC CC-3', Dcaf7-reverse: 5'-TTA GCT GTC AGG AAA CCT GAC CC-3'; Trim56-forward: 5'-ATG AAC TCC AAA GTC TCC TCC CC-3', Trim56-reverse: 5'-TTA GCT GTC AGG AAA CCT GAC CC-3'; Otud4-forward: ATG

GAG GCA GCC GTC GGC-3', Otud4-reverse: 5'-TTA AGT GTG TTG TCC CCT GTG GCC-3'; Rc3h1-forward: 5'-ATG CCT GTA CAA GCT CCA CAA TG-3', Rc3h1-reverse: TTA AGG AGC AGA ACT GGG AGT AAC-3'; Rnf214-forward: 5'-ATG GCA GCG TCT GAG GTT GC-3', Rnf214-reverse: 5'-TCA TTT AAG AGT TGG ACA AAA GGG AC-3'. The human Otud4 isoform lacking the N-terminal catalytic domain (Otud4-Δ) was cloned in the pCAGIG vector from the MGC cDNA (Horizon: MHS6278-211690330) using primers, hOtud4delta-forward: 5'-ATG GCC TGT ATT CAC TAT CTT CG-3' and hOtud4delta-reverse: 5'-TCA AGT GTG CTG TCC CCT ATG G-3'. The myc tag was introduced at the C-terminus of each gene by PCR with primers comprising the myc sequence and subcloned into the pcDNA3 and pCAGIG vectors (Addgene #11159). To generate shRNAs against mouse Otud4, double-stranded oligonucleotides encoding shRNA sequences (Life Technologies) were cloned into the pSUPER vector. The shRNA sequences used were shRNA-1 (GCG TTT ATA GAA GGG TCA T), shRNA-2 (GCA TGC ATT CTC CAG TCA T), shRNA-3 (GCT TCT TCA TGC TGA ATA T). An shRNA against luciferase was used as a control. All clones were verified by sequencing. pCMV6-DDK-DDX6 was purchased from Origene (MR207739). pRK5-HA-Ubi (#17608), pRK5-HA-Ubi K0 (#17603), pT7-EGFP-C1-HsDCP1a (#25030), pCDNA3-FLAG-hDCP2 (#72213) and pT7-EGFP-C1-HsNOT7 (#37325) were purchased from Addgene.

3.7 Ubiquitination immunoprecipitation: For immunoprecipitation, antibody-beads mix was prepared by washing 50 µL Protein A/G magnetic beads (Bio-Rad #1614013,1614023) per sample twice with RIPA buffer (50 mM Tris-HCl, 150 mM NaCl, 2 mM EDTA, 1% Triton-X topped up to 50 mL with water). The beads were then incubated with 2-3 µg of antibody at room temperature for 30 minutes. The cells were first washed with ice-cold PBS twice. To lyse cells, 300 µL of lysis buffer (RIPA buffer supplemented with 1X Phenylmethylsulphonyl

Fluoride (PMSF) (Sigma #329986), 50 mM N-Ethylmaleimide (Sigma #123530) and 1X Halt protease and phosphatase inhibitor) (Thermofisher Scientific #PI78443)and was added to each 10 cm dish. Cells were incubated for 10 minutes on ice and were collected using a cell scraper. To lyse cells, sonication (QSonica, Q125) was used at 50% power for 10 seconds thrice with intermediate 10 seconds incubation on ice. The cell lysate was then centrifuged at maximum speed (~20,000 X g) for 10 minutes at 4ºC and the supernatant was collected. 0.1% SDS (Biobasic #SD8118) was added to the cell lysate. To reduce non-specific binding, the cell lysate was precleared using 20 µL beads for 30 minutes at 4ºC. Following the incubation, 10 µL of lysate was taken as input and the remaining was incubated with the antibody-beads mix for three hours. The beads were then washed thrice with RIPA buffer containing 0.1% SDS for 15 minutes each at 4ºC. To elute the bound proteins, beads were boiled at 100ºC for 5 minutes in 2X Laemmli Buffer containing 200 mM dithiothreitol (DTT) (Sigma #3483123) and analysed by SDS-PAGE.

3.8 Co-immunoprecipitation: To analyse protein-protein interactions co-immunoprecipitation was used as it helps to not only pull-down target protein, but also any other protein interacting with it. Cells were lysed with gentle lysis buffer (2.5 mM Tris-HCl, 10 mM NaCl, 2 mM EDTA, 1 mM EGTA, 0.5% Triton-X, 10% glycerol) supplemented with 1X PMSF and 1X Halt protease and phosphatase inhibitor. Similar steps were followed as ubiquitination immunoprecipitation. To prevent loss of protein interactions detergents like SDS were not used.

3.9 Denaturing immunoprecipitation: Compared to standard immunoprecipitation, wherein the antigen is recognized by the antibody in native form, in denaturing immunoprecipitation the antibody recognizes denatured proteins. Denaturing immunoprecipitation breaks protein

interactions, therefore, preventing any artefacts that may arise due to the pull down of any interacting protein. For the denaturing immunoprecipitation, antibody-beads mix were prepared as mentioned above. Cells were washed with PBS twice and then lysed using 100µL gentle lysis buffer containing 5% glycerol. Cells were incubated on ice, lysed using sonication and the lysate was centrifuged as mentioned above. SDS was added to 1% and the supernatant was denatured by boiling at 100°C for 5 minutes. The lysate was diluted to 0.1% SDS by addition of SDS free lysis buffer. This was then incubated with beads to remove non-specific binding and the same procedure was followed as mentioned above.

3.10 Western Blot: Samples were loaded on SDS-PAGE gels (6-10%) and run at the following conditions: 80V for 20 minutes, 120V for 120 minutes. After electrophoresis proteins were transferred to nitrocellulose membrane overnight at 32V. The membrane was blocked using 5% BSA in TBS-T for one hour at room temperature and incubated with primary antibody diluted in 5% BSA in TBS-T overnight. On the following day, membrane was washed thrice for 15 minutes each with 1X TBS-T and incubated with HRP-conjugated secondary antibody (Thermofisher Scientific #G-21234, #a16023) (Abcam #ab6808) diluted in PBS for 1 hour and room temperature. The membrane was then washed thrice with 1X TBS-T, analysed using ECL substrate (Sigma #RPN2109), imaged using Amersham Imager 600 and quantified using ImageJ.

3.11 Immunostaining and confocal microscopy: For immunostaining HEK293 cells and NPCs, cells were first washed thrice with 1X PBS and fixed with 4% paraformaldehyde (PFA) (Electron Microscopy Sciences #15710) for 15 minutes at room temperature. Cells were then washed thrice with 1X PBS and permeabilised using 0.3% Triton-X/PBS for 10 minutes. Cells were blocked 5% Normal Donkey Serum (NDS) (Sigma #S30-M) in PBS for 1 hour, followed

by incubation with primary antibody diluted in 5% NDS/PBS for 1 hour at room temperature. Following this, cells were washed thrice with 1X PBS and incubated with appropriate secondary antibodies at room temperature for one hour. The cells were then washed thrice with 1X PBS. Nuclei were stained using Hoechst 33258 (1:1000 dilution) (Thermofisher Scientific #H3569). Coverslips were mounted on glass slides with Aqua-Poly/Mount (Polysciences #18606-20). Cells were imaged at 60X objective using Olympus FV3000 confocal microscope and quantified using ImageJ.

3.12 Statistical analysis: Immunocytochemistry results are presented as scatter plots with mean. Western blot quantifications are depicted as bar graphs with mean. Error bars depict standard error of the mean. All statistical analysis was performed on GraphPad Prism.

Chapter 4

To assess the ubiquitination of 4E-T and its correlation with PB assembly.

Processing bodies (P-bodies) are RNA-protein granules (RNPs) formed by a series of dense network of multivalent RNA-protein interactions (Hubstenberger et al., 2017). Previous research has hinted at the role of post-translational mechanisms such as ubiquitination in regulating dynamics of membrane-less organelles (Bah and Forman-Kay, 2016). For instance, P-body (PB) proteins were found to be enriched in lysine residues and lysine is often post-translationally modified by ubiquitin. Additionally, a general knock down of ubiquitin resulted in decrease in PB assembly within the cell, raising the possibility that post-translational ubiquitination serves as a molecular signaling mechanism that regulates PB assembly (Tenekeci et al., 2016; Ukmar-Godec et al., 2019). Here, we will first assess the role of ubiquitination on PB assembly and dissect the underlying mechanisms.

4.1 Ubiquitination is critical for PB assembly

To assess the role of ubiquitination on PB assembly, the impact of inhibition of ubiquitination on PB assembly was investigated. To this end, cortical NSC culture was prepared from E12.5 mouse embryos and treated with 1 μM [(1R,2R,3S,4R)-2,3-dihydroxy-4-[[2-[3-[(trifluoromethyl)thio]phenyl]pyrazolo[1,5-a]pyrimidin-7-yl]amino]cyclopentyl]sulfamic acid methyl ester (commonly known as TAK-243 or MLN7243), an E1-activating enzyme inhibitor, for 4 hours (Hyer et al., 2018; Markmiller et al., 2019). Neural stem cells were immunostained for PB proteins 4E-T and EDC4. It is expected that if ubiquitination is critical for PB assembly, inhibition of ubiquitination should result in a corresponding decrease in the number of PBs.

In NSC treated with DMSO (control), cytoplasmic foci positive for PB markers 4E-T and EDC4 were detected. Following TAK-243 treatment in neural stem cells, a diffused cytoplasmic expression was observed for PB markers 4E-T and EDC4. 4E-T and EDC4 double positive foci were quantified and a ~60% reduction was observed in PB foci following TAK-243 treatment **(Figure 8).** The decrease in number of PBs following TAK-243 treatment suggests a potential role of ubiquitination as a signaling mechanism regulating PB dynamics.

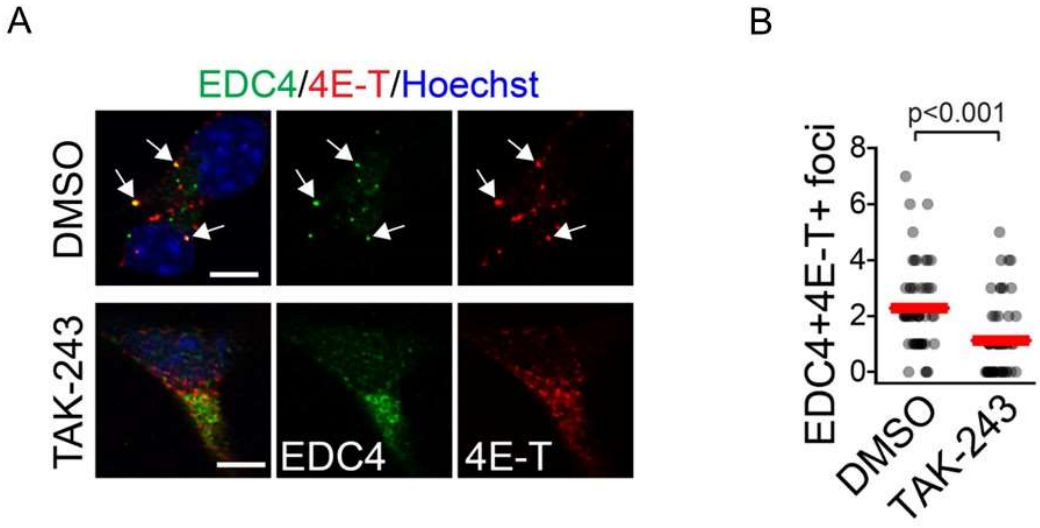

Figure 8. Ubiquitination is critical for PB assembly.

(A) E12.5 neural stem cells were treated with either control (DMSO) or TAK-243 and immunostained for 4E-T (red) and EDC4 (green). Cells were counterstained with Hoechst. Arrows indicate foci positive for both 4E-T and EDC4. Scale bar is 5 µm.

(B) Quantification for number of 4E-T and EDC4 double positive foci. Each dot represents a cell, and the crossbar indicates the mean. Mann-Whitney test. n=50 cells each.

4.2 Core PB proteins are ubiquitinated.

While previous experiment with ubiquitin activating enzyme inhibitor, TAK-243 suggests the role of ubiquitination in regulating PB dynamics, the exact molecular targets and underlying molecular mechanisms remain unknown. I speculated that ubiquitination of certain core PB protein(s) regulate PB dynamics.

To delineate the relevant molecular targets, ubiquitination of core PB proteins such as mRNA decapping enzyme 1A (DCP1a), mRNA decapping enzyme 2 (DCP2), CCR-NOT transcription complex subunit 7 (CNOT7), DNA topoisomerase 3b (TOP3b) and eukaryotic translation initiation factor 4E transporter (4E-T) was analysed. To answer whether PB proteins were ubiquitinated, each individual protein was overexpressed in HEK293 cells with and without HA-Ubiquitin. Since, HA is not endogenously expressed in HEK293 cells, ectopic expression of tagged ubiquitin allows to differentiate ubiquitination bands from non-specific bands on the western blot. As the ubiquitination mechanism is conserved across all cell types, HEK293 cells were used as these cells can easily be transfected and additionally are flat, making analysis of PBs easier. The cells were lysed, target protein was immunoprecipitated, analysed by SDS-PAGE and probed with HA (ubiquitin).

Analysis of core PB proteins revealed that DCP1a, DCP2, CNOT7 and TOP3b were poly-ubiquitinated as evident by the poly-ubiquitination ladder observed in western blot **(Figure 9)**. Intriguingly, it was found that 4E-T displayed a single ubiquitination band that migrated slower than the 4E-T band **(Figure 10A)**. The band was ~10 kDa higher than 4E-T, consistent with the size of a single ubiquitin molecule, indicating monoubiquitination of 4E-T. It is also worthy to note that the two bands present on immunoblot V5 are phosphorylation bands depicting that 4E-T is hyperphosphorylated (data not shown).

Monoubiquitination of 4E-T is of particular interest for the following three reasons: First, 4E-T is a core PB protein important for PB assembly (Ferraiuolo et al., 2005). Second,

4E-T is a critical regulator for stem cell homeostasis, wherein 4E-T helps maintain a steady stem cell pool by preventing premature neuronal differentiation (Yang et al., 2014). Third, monoubiquitination often serves signaling functions in the cell. Therefore, the remainder of the study focuses on delineating the effect of monoubiquitination of 4E-T on PB assembly.

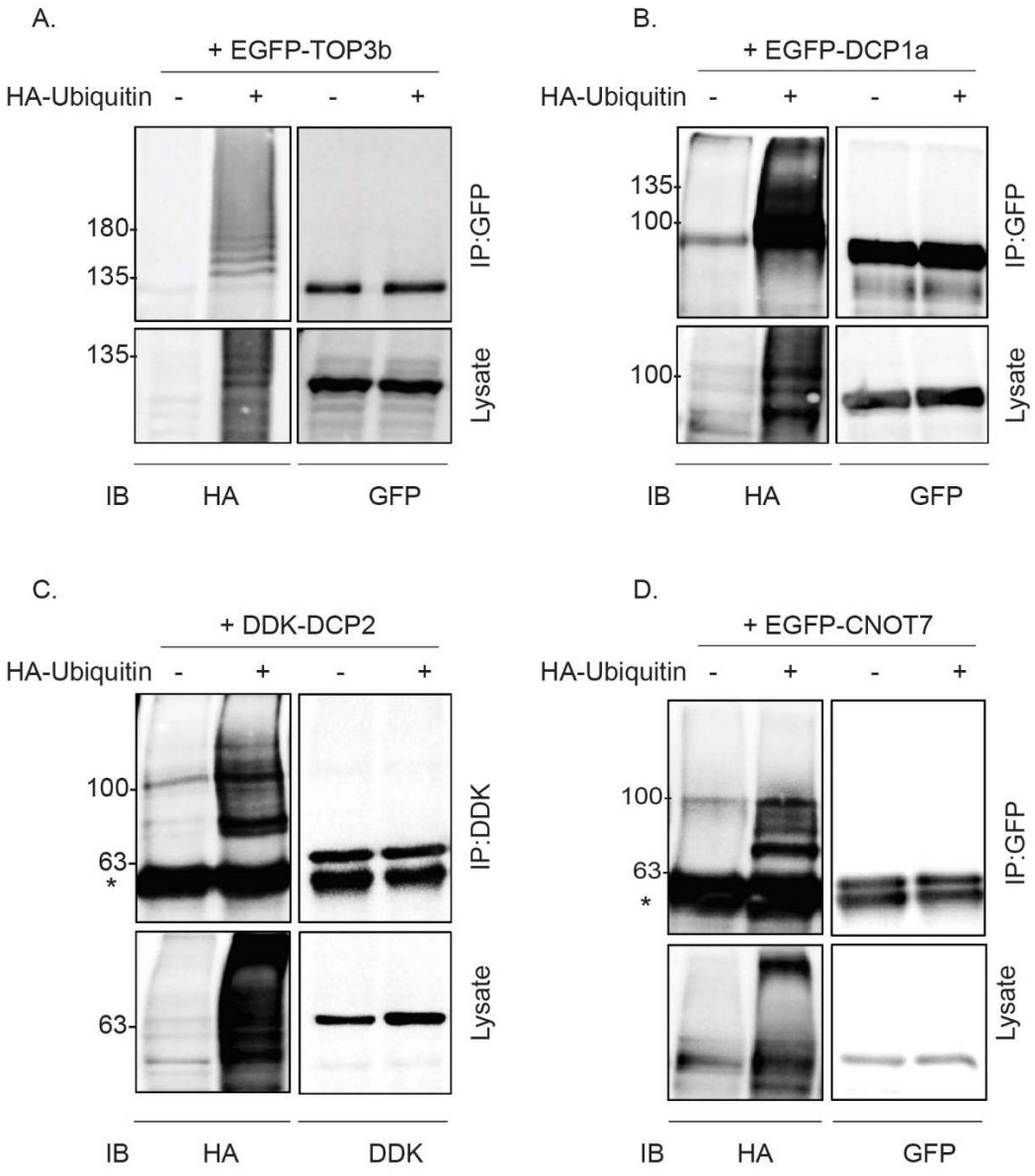

Figure 9. Core PB proteins are ubiquitinated.

(A-D). Immunoprecipitation of HEK293 cells transfected with epitope-tagged target protein with and without HA-Ubiquitin. Western blot analysis shows polyubiquitination of (A) TOP3b, (B) DCP1a, (C) DCP2 and (D) CNOT7. Lysate input represents 1.5% of total cell lysate prior to immunoprecipitation. Results are representative of three independent experiments. * indicates IgG heavy chain band.

4.3 4E-T is monoubiquitinated.

To further assess if 4E-T ubiquitination regulates PB dynamics, additional experiments were carried out to first confirm the ubiquitination of 4E-T and second to further confirm its monoubiquitination.

4.3.1 4E-T is ubiquitinated:

To confirm if the ubiquitination band observed was not due to non-specific binding of the HA tag or non-specific interaction with other ubiquitinated proteins, the following four experiments were performed: To confirm that the epitope tag is not a factor affecting ubiquitination, ubiquitination assay of 4E-T was repeated using EGFP-4E-T. 4E-T was immunoprecipitated using GFP antibody, analysed by SDS-PAGE and probed with HA (ubiquitin) and GFP (4E-T). A single ubiquitination band was observed that migrated ~10 kDa slower than the 4E-T band, confirming the specificity of the ubiquitination band observed before **(Figure 10B).**

Denaturing immunoprecipitation was used to further confirm ubiquitination of 4E-T. Unlike standard ubiquitination immunoprecipitation, denaturing immunoprecipitation involves boiling proteins at 100º C for 5 minutes in presence of SDS. This denatures the proteins and breaks all protein-protein interactions, allowing antibody to identify and pull-down the target protein only, preventing experimental artefacts from pull-down of any other interacting partner. Similar to ubiquitination immunoprecipitation, denaturing immunoprecipitation was performed for both EGFP/V5 tagged 4E-T, was analysed by SDS-PAGE and probed with EGFP/V5 or HA antibodies**.** A single ubiquitination band, similar to previous experiments, was observed under denaturing conditons, confirming that the ubiquitination band observed was specific to 4E-T and not due to any other interacting protein **(Figure 10C, D)**.

Additionally, ubiquitin attaches to the substrate generally via a lysine and rarely through a methionine residue (Akutsu et al., 2016). To further confirm the specificity of the ubiquitination band, 4E-T KR, a mutant form of 4E-T was used, wherein all lysine residues were mutated to arginine, preventing ubiquitination of 4E-T via a lysine (Petroski and Deshaies, 2005). Since lysine to arginine mutation can affect protein structure and stability, this experiment was only used as a quick preliminary confirmation of 4E-T ubiquitination. HEK293 cells were transfected with EGFP-4E-T WT with and without HA-Ubiquitin as well as EGFP-4E-T KR with and without HA-Ubiquitin, immunoprecipitated with EGFP antibody and analysed using SDS-PAGE. A loss of ubiquitination band was observed for 4E-T KR, confirming that 4E-T is ubiquitinated via a lysine **(Figure 10E)**.

Furthermore, to confirm ubiquitination of 4E-T, HEK293 cells were transfected with V5-4E-T with and without HA-Ubiquitin. Transfected cells were either treated with DMSO (control) or 1 µM TAK-243 and immunoprecipitated for 4E-T. The pulled down proteins were analysed using SDS-PAGE and immunoblotted for V5 (4E-T) and HA (ubiquitin). ~70%

decrease in intensity of ubiquitination band was observed following TAK-243 treatment, confirming that the band observed in Figure 5 is specific to ubiquitination **(Figure 11)**.

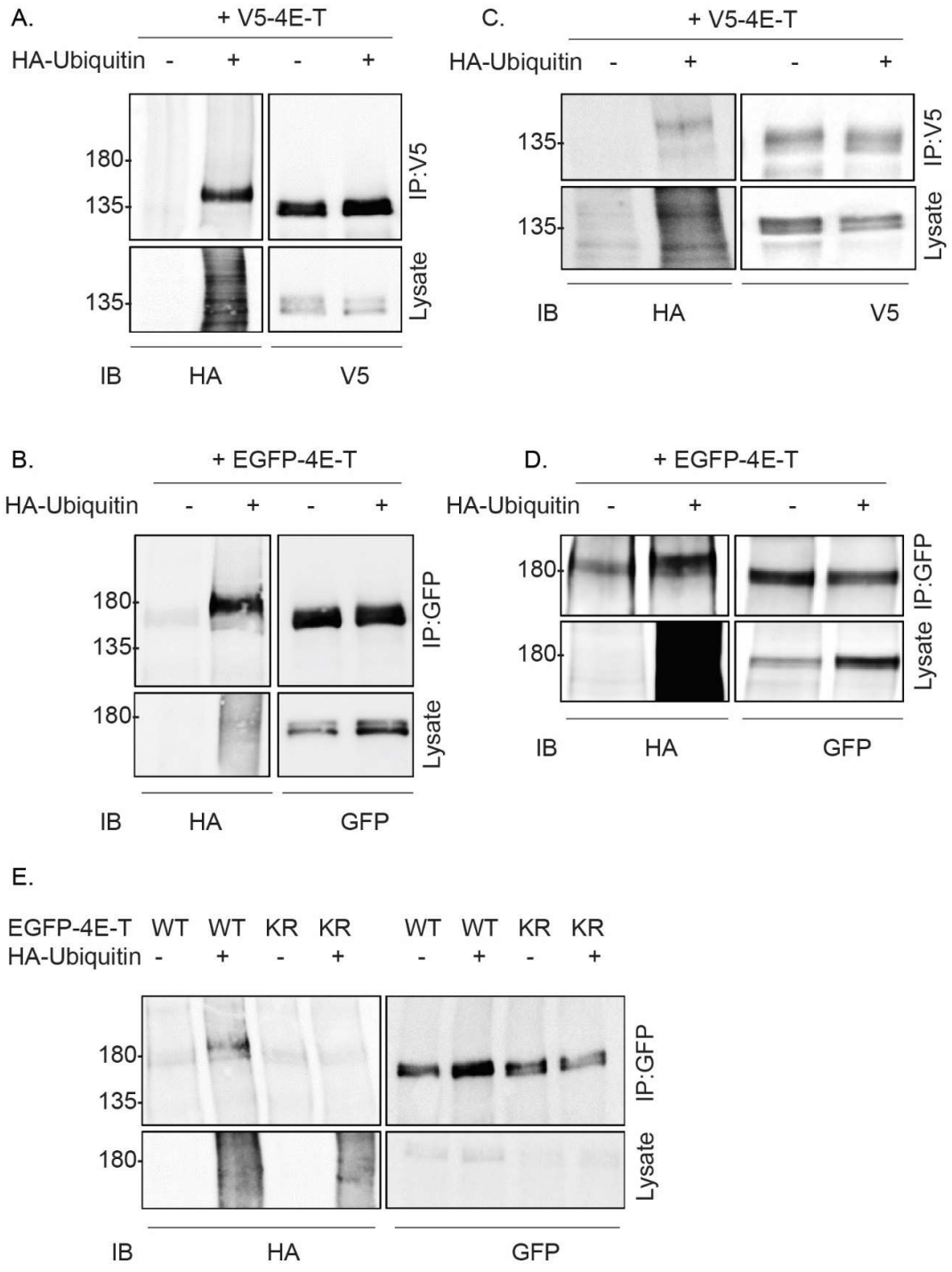

Figure 10. 4E-T is ubiquitinated.

(A). Immunoprecipitation (IP, with anti-V5) of HEK293 cells transfected with V5-4E-T with and without HA-Ubiquitin. Western blot analysis shows a single ubiquitination band, indicating monoubiquitination of 4E-T.

(B). Immunoprecipitation (with anti-GFP) of HEK293 cells transfected with EGFP-4E-T with and without HA-Ubiquitin. Western blot analysis confirms monoubiquitination of 4E-T.

(C). Denaturing immunoprecipitation (with anti-V5) of HEK293 cells transfected with V5-4E-T with and without HA-Ubiquitin. Western blot analysis confirms monoubiquitination of 4E-T under denaturing conditions.

(D). Denaturing immunoprecipitation (with anti-GFP) of HEK293 cells transfected with EGFP-4E-T with and without HA-Ubiquitin. Western blot analysis shows monoubiquitination of 4E-T under denaturing conditions.

(E). Immunoprecipitation (with anti-GFP) of HEK293 cells transfected with either EGFP-4E-T WT or EGFP-4E-T KR with and without HA-Ubiquitin. Western blot analysis shows lack of monoubiquitination for 4E-T KR.

Lysate input represents 1.5% of total cell lysate prior to immunoprecipitation. Results are representative of three independent experiments.

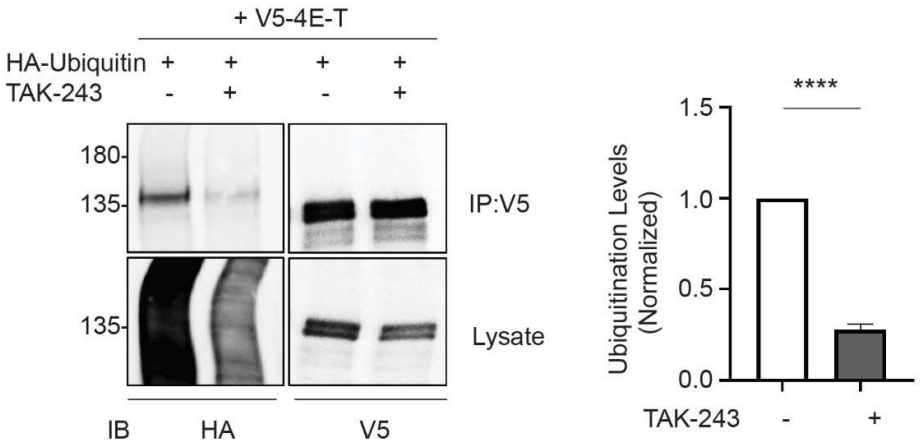

Figure 11. Loss of 4E-T ubiquitination with TAK-243 treatment confirms specificity of ubiquitination band. (A). Immunoprecipitation (with anti-V5) with V5-4E-T only, V5-4E-T with HA-Ubiquitin. HEK293 cells were treated with either control (DMSO) or E1-activating enzyme inhibitor, TAK-243. Western blot analysis confirmed decrease in intensity of monoubiquitination band with TAK-243 treatment. 4E-T ubiquitination levels were normalized to V5-4E-T levels. Quantification of relative 4E-T ubiquitination levels by normalizing the intensity of 4E-T ubiquitination levels with TAK-243 treatment to control. Statistical analysis was performed using Student's two-tailed t test. Error bars denote SEM. ****$p < 0.0001$ for n=3 experiments.

Lysate input represents 1.5% of total cell lysate prior to immunoprecipitation. Results are representative of three independent experiments.

4.3.2 4E-T is monoubiquitinated.

To confirm monoubiquitination of 4E-T the following two methods were used. For the first experiment, HEK293 cells were transfected with V5-4E-T with and without HA-

Ubiquitin. Transfected cells were treated with 10 μM MG132, a proteasome inhibitor for 4 hours and 4E-T was immunoprecipitated using V5 antibody (Moriwaki and Chan, 2016) **(Figure 12A)**. Monoubiquitination of 4E-T might serve as a precursor for polyubiquitination or polyubiquitin ladder of 4E-T might be rapidly degraded, therefore inhibiting the proteasome will help ascertain if 4E-T is polyubiquitinated.

Following MG132 treatment, only a single ubiquitination band was again observed ~10kDa higher than the 4E-T band, confirming that 4E-T is not polyubiquitinated **(Figure 12A)**. Additionally, a decrease in intensity of the ubiquitination band of 4E-T was observed following MG132 treatment, most likely due to the inability of cells to recycle ubiquitin leading to a decrease in overall availability of free ubiquitin.

For the second experiment HEK293 cells were transfected with V5-4E-T with either HA-Ubiquitin WT or HA-Ubiquitin K0, a mutant form of ubiquitin where all lysine residues are mutated to arginine. Since the glycine of ubiquitin (G76) forms the first attachment with lysine of the substrate, use of HA-Ubiquitin K0 will still allow for attachment of one ubiquitin moiety (Petroski and Deshaies, 2005; Taal et al., 2019). However, since the attachment of any additional ubiquitin occurs via the lysine, the use of HA-Ubiquitin K0 will prevent chain growth. The transfected HEK293 cells were incubated for 48 hours, immunoprecipitated for 4E-T and analysed using SDS-PAGE **(Figure 12B)**.

Similar to HA-Ubiquitin WT, a single ubiquitination band was observed for HA-Ubiquitin K0, confirming monoubiquitination of 4E-T **(Figure 12B)**. Additionally, an increase in intensity of the ubiquitination band was observed with HA-Ubiquitin K0, most likely due to the inability of mutant ubiquitin to form polyubiquitin linkages with other substrates leading to an increase in overall ability of free ubiquitin in the cell.

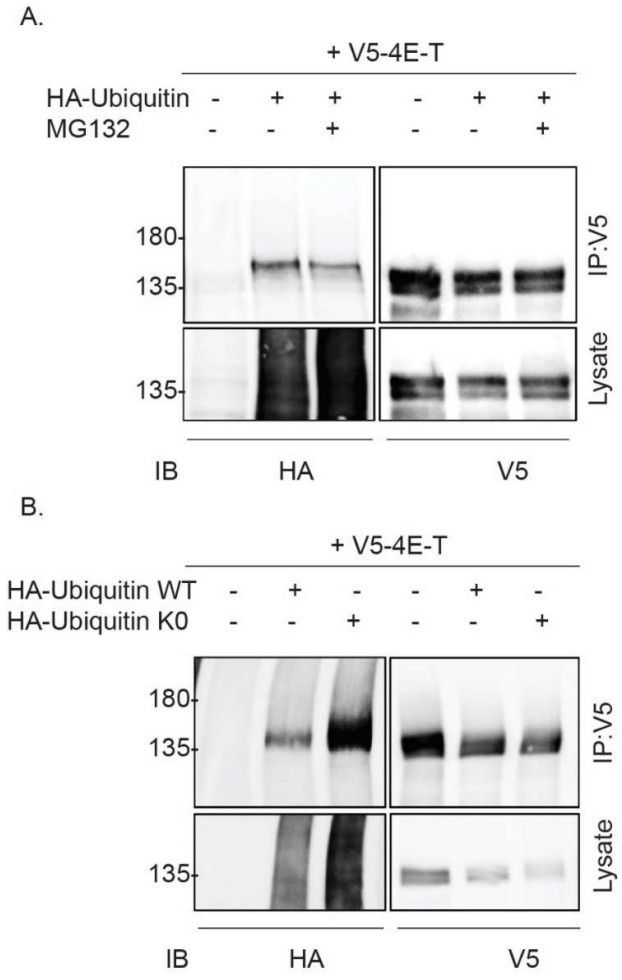

Figure 12. 4E-T is monoubiquitinated.

(A). Immunoprecipitation (with anti-V5) of HEK293 cells transfected with V5-4E-T with and without HA-Ubiquitin. HEK293 cells were treated with either control (DMSO) or proteasome inhibitor (MG132). Western blot analysis confirms absence of polyubiquitination ladder with MG132 treatment.

(B). Immunoprecipitation (with anti-V5) of HEK293 cells transfected with V5-4E-T only, V5-4E-T with either HA-Ubiquitin WT and HA-Ubiquitin K0. Western blot analysis confirms presence of a single monoubiqutination band with both Ubiquitin-WT and Ubiquitin-K0.

Lysate input represents 1.5% of total cell lysate prior to immunoprecipitation. Results are representative of three independent experiments.

4.4 4E-T ubiquitination correlates with PB assembly.

Since previous experiments confirmed monoubiquitination of 4E-T, the next step was to determine how 4E-T monoubiquitination regulates PB assembly. Therefore, to assess if monoubiquitination of 4E-T correlates with PB assembly, HEK293 cells were transfected with EGFP-4E-T with and without HA-Ubiquitin and treated with 10 µg/mL cycloheximide for 1 hour at 37ºC. Cycloheximide is a translation inhibitor that blocks eukaryotic elongation process (Schneider-Poetsch et al., 2010). Since formation of RNP granules like PBs is dependent on presence of free RNA, treatment with cycloheximide reduces PB assembly by trapping mRNA on polysomes (Lui et al., 2014; Teixeira et al., 2005). The cells were lysed, and 4E-T was immunoprecipitated and analyzed using SDS-PAGE. As a control, cells were treated with dimethyl sulfoxide (DMSO) and the ubiquitination band intensity between control and cycloheximide-treated samples was quantified and compared using ImageJ. Following cycloheximide treatment, a reduction in the ubiquitination band intensity was observed by about 50% **(Figure 13A)**.

Alternatively, HEK293 cells were transfected with EGFP-4E-T with and without HA-Ubiquitin and treated with 20 µg/mL puromycin for 3 hours at 37ºC. Puromycin is a translation inhibitor that causes release of nascent polypeptides and ribosomes from mRNA, resulting in a subsequent increase in PB assembly (Eulalio et al., 2007b; Yan et al., 2016). The cells were lysed and immunoprecipitated for 4E-T and analysed using SDS-PAGE by immunoblotting for HA (Ubiquitin). The ubiquitination band intensities between DMSO-treated (control) and

puromycin-treated were quantified and analysed using ImageJ. It was observed that increase in number of PBs with puromycin resulted in a corresponding increase in the intensity of the ubiquitination band by 60% **(Figure 13B)**.

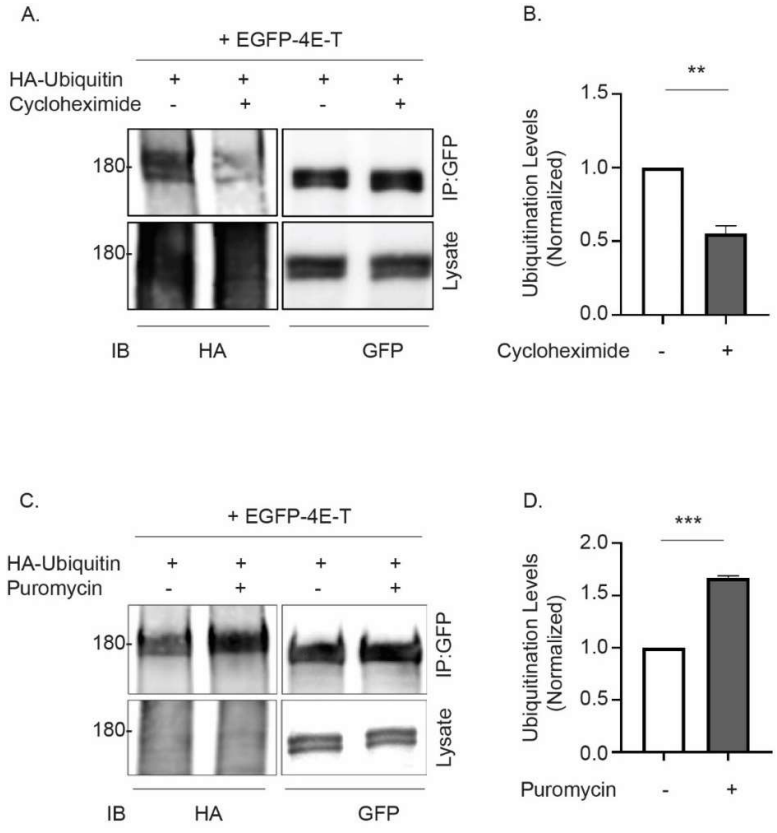

Figure 13. 4E-T monoubiquitination correlates with PB formation.

(A). Immunoprecipitation (with anti-GFP) of HEK293 cells transfected with EGFP-4E-T with HA-Ubiquitin. HEK293 cells were treated with either DMSO (control) or 10 µg/ml cycloheximide for 1 hour. Western blot analysis confirms decrease in intensity of ubiquitination band with cycloheximide treatment.

(B). 4E-T ubiquitination levels were normalized to V5-4E-T levels. Quantification of relative 4E-T ubiquitination levels by normalizing the intensity of 4E-T ubiquitination levels with

cycloheximide treatment to control. Statistical analysis was performed using Student's two-tailed t test. Error bars denote SEM. **p=0.0011 for n=3 experiments.

(C). Immunoprecipitation (with anti-GFP) of HEK293 cells transfected with EGFP-4E-T with HA-Ubiquitin. HEK293 cells were treated with either DMSO (control) or 20 µg/ml puromycin for 3 hours. Western blot analysis confirms decrease in intensity of ubiquitination band with puromycin treatment.

(D). Quantification of relative 4E-T ubiquitination levels by normalizing the intensity of 4E-T ubiquitination levels with puromycin treatment to control. Statistical analysis was performed using Student's two-tailed t test. Error bars denote SEM. **p=0.0009 for n=3 experiments.

Lysate input represents 1.5% of total cell lysate prior to immunoprecipitation. Results are representative of three independent experiments.

4.5 Summary

This Chapter first confirms that 4E-T ubiquitination is critical for PB assembly. Inhibition of ubiquitination using E1 activating enzyme inhibitor TAK-243 resulted in a loss of PBs, suggesting ubiquitination is an important regulator of PB dynamics. To further delineate the molecular targets and the exact molecular mechanism, ubiquitination of some key PB proteins was assessed and it was found that 4E-T, a core PB protein is monoubiquitinated. This monoubiquitination of 4E-T was confirmed using various biochemical approaches and it was found that 4E-T monoubiquitination levels change corresponding to PB numbers, indicating that 4E-T ubiquitination correlates with PB assembly.

Chapter 5

To examine the molecular process monoubiquitination of 4E-T regulates PB assembly

5.1 Monoubiquitination of 4E-T is required for its targeting to PBs.

Monoubiquitination of 4E-T can either be due its presence in PBs or can alternatively drive partitioning of 4E-T into PBs triggering their assembly. To address this question, EGFP-4E-T WT and mutant EGFP-4E-T KR, wherein all lysines are mutated to arginines preventing ubiquitination, will be transfected in HEK293 cells and immunostained for EGFP. It is expected that if 4E-T ubiquitination is required for its targeting to PBs, a decrease in EGFP positive cytoplasmic foci will be observed for 4E-T KR in comparison to 4E-T WT.

In HEK293 cells transfect with EGFP-4E-T WT distinct cytoplasmic foci were observed, compared to 4E-T KR, where 4E-T was diffusely expressed throughout the cytoplasm. These EGFP-positive foci were quantified and a ~50% decrease was observed with 4E-T KR confirming that ubiquitination is required for its targeting to PBs **(Figure 14 A,B)**.

5.2 Monoubiquitination of 4E-T is required for PB assembly

Previous experiments have explained that monoubiquitination of 4E-T is required for its targeting to PBs. To next assess if this monoubiquitination is required for endogenous PB assembly, HEK293 cells were transfected with EGFP-4E-T WT and EGFP-4E-T KR and immunostained for endogenous PB markers such as EDC4 and DCP1a.

HEK293 cells transfected with EGFP-4E-T WT showed distinct cytoplasmic EGFP positive foci. Immunostaining with endogenous PB markers EDC4 and DCP1a showed a strong overlap, confirming that 4E-T WT can assemble into PBs. On the other hand, a decrease a number of cytoplasmic foci was observed for 4E-T KR with little/no overlap with endogenous

PB markers DCP1a and EDC4, confirming that ubiquitination of 4E-T is required for PB assembly **(Figure 14).** This decrease in endogenous PBs also suggests that 4E-T KR functions in a dominant-negative manner to suppress PB formation.

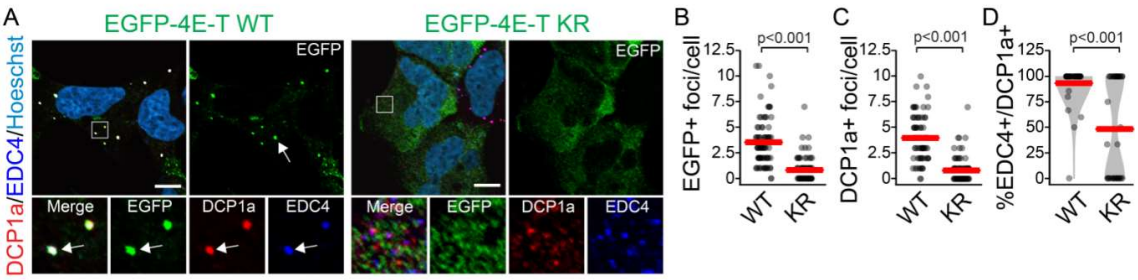

Figure 14. 4E-T ubiquitination drives PB assembly.

HEK293 cells were transfected with either EGFP-4E-T WT or EGFP-4E-T KR and (A) immunostained for EGFP (4E-T), DCP1a and EDC4. Arrows indicate marker positive foci. Cells were quantified for the number of (B) EGFP positive foci per cell (C) DCP1a positive foci per cell (D) percentage of EDC4 and DCP1a double positive foci. Each dot represents a cell, and the crossbar indicates the mean. Cells were counterstained with Hoechst. Statistical analysis using Mann-Whitney test. ****p<0.001, ****p<0.001. Scale bar is 5 µm.

Furthermore, to confirm if the effects observed on PBs were due to ubiquitination, or due to other post-translational modifications via lysine, HEK293 cells were transfected with 4E-T ubiquitin fusion mimic. The ubiquitin mimic (Ub-4E-T) contains one ubiquitin fused to N-terminus of 4E-T KR to mimic monoubiquitination of 4E-T. HEK293 cells were transfected

with either V5-4E-T or V5-Ub-4E-T, immunostained for V5 and PB markers DCP1a and EDC4 and quantified for the number of PBs observed.

Immunostaining HEK293 cells transfected with V5-Ub-4E-T showed a rescue in the number of V5-postive as well as EDC4 and DCP1a double positive foci, confirming that the loss of PBs observed for 4E-T KR was specific to ubiquitination. Closer examination also revealed an increase in the number of PBs with smaller sizes, which are rarely seen in 4E-T WT cells **(Figure 15)**. These results indicate that while 4E-T ubiquitination is sufficient to drive PB assembly, excessive ubiquitination can result in its remodelling.

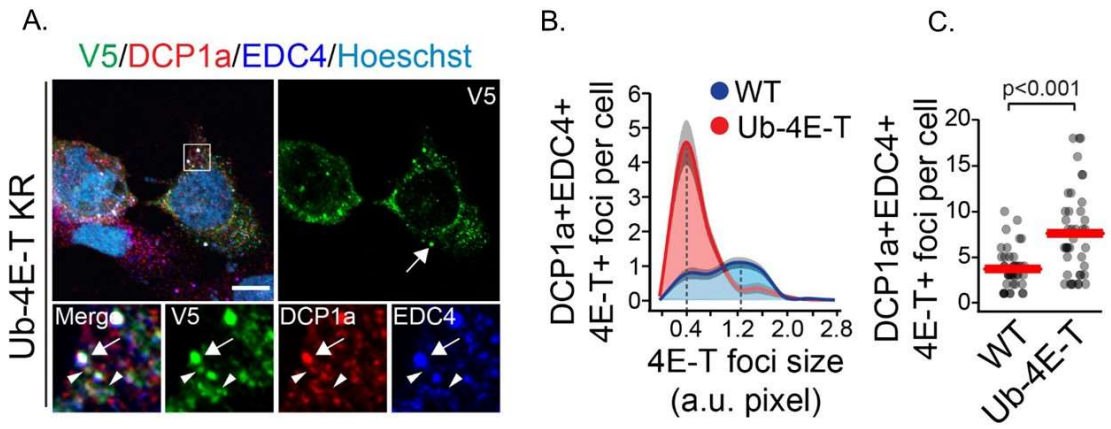

Figure 15. 4E-T ubiquitination is required for PB assembly.

HEK293 cells were transfected with either V5-4E-T WT or V5-Ub-4E-T KR and (A) immunostained for V5 (4E-T), DCP1a and EDC4. Arrows indicate marker positive foci. Cells were quantified for (A) size of 4E-T foci and (B) the number of EDC4 and DCP1a double positive foci. Each dot represents a cell, and the crossbar indicates the mean. Cells were counterstained with Hoechst. Statistical analysis using Mann-Whitney test. ****p<0.001. Scale bar is 5 µm.

5.3 Monoubiquitination of 4E-T drives multi-step assembly of PBs

PBs assemble through a series of multivalent interactions resulting in a dense cluster of protein-protein and RNA-protein network (Hubstenberger et al., 2017; Rao and Parker, 2017). PBs might assemble through the following two methods: First, monoubiquitination of 4E-T can drive simultaneous one-step assembly of PBs, based on which loss of ubiquitination will result in loss of all interactions between 4E-T and other PB proteins. Second, monoubiquitination of 4E-T can signal a sequential multi-step assembly of PBs, wherein there exists several smaller clusters of protein networks, which on 4E-T ubiquitination assemble together to form a functional PB. Based on this model, loss of 4E-T ubiquitination will still preserve some interactions between 4E-T and other PB proteins but will prevent their assembly into a functional PB. Mechanistically, it is therefore critical to understand how 4E-T monoubiquitination alters protein interaction networks to drive PB assembly.

5.3.1 Loss of ubiquitination results in changes in 4E-T interaction networks

To delineate the mechanistic steps of PB assembly 4E-T interaction networks with and without monoubiquitination were analysed. HEK293 cells were transfected with either EGFP-4E-T WT or EGFP-4E-T KR and 4E-T was co-immunoprecipitated using EGFP antibody. Compared to standard immunoprecipitation, co-immunoprecipitation also pulls down any protein interacting with 4E-T. The pulled down proteins were later analysed using mass spectrometry, performed at the core facility (Southern Alberta Mass Spectrometry Facility, Cumming School of Medicine, University of Calgary). Bioinformatic analysis for the mass spectrometry results were performed by Xin Chen (Yang lab) **(Figure 16)**.

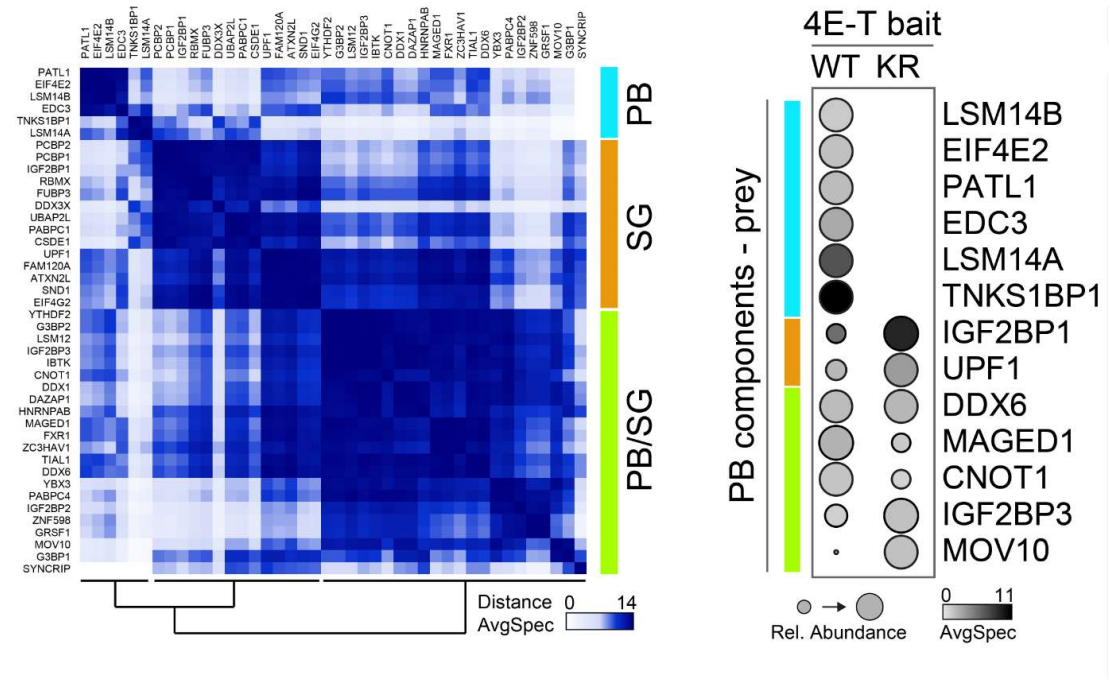

Figure 16. Analysis of 4E-T interaction networks for PB assembly in HEK293 cells.

HEK293 cells were transfected with either EGFP-4E-T WT or EGFP-4E-T KR and immunoprecipitated for 4E-T (bait) using GFP antibody. A total of 49 PB and SG proteins (confidence score >12 in the RNA Granule Database, http://rnagranuledb.lunenfeld.ca/) with a spectral count greater than 2 in at least two out of three replicates in either 4E-T WT or 4E-T KR groups were selected for the analysis. Canberra distance matrix of prey proteins based on the average spectral count was generated. (A) Heat map showing distance between 4E-T interactors as identified by mass spectrometry. (B) Dot plot showing differential interactors of PB proteins with 4E-T WT or 4E-T KR. Bioinformatic analysis for mass spectrometry results was performed by Xin Chen.

Group 1: Loss of PB protein interactions with 4E-T KR
• LSM14A • LSM14B • EIF4E2 • PATL1 • EDC3 • TNKS1BP1

Table1: PB proteins interacting with 4E-T WT but not 4E-T KR.

Group 2: PB proteins interacting with both 4E-T WT and 4E-T KR
• IGF2BP1 • UPF1 • DDX6 • MAGED1 • CNOT1 • IGF2BP3 • MOV10

Table 2: PB proteins interacting with both 4E-T WT and 4E-T KR.

Expectantly, co-immunoprecipitation of 4E-T WT pulled down several PB proteins such as DDX6, EDC3, CNOT1 as well as several proteins such as CSDE1, G3BP1 associated

with stress granules, another type of membrane-less RNP granule present in the cytoplasm (Hubstenberger et al., 2017; Kedersha et al., 2005; Sanders et al., 2020). Unlike PBs, stress granules are not constitutive and are generally induced on cellular stress such as heat shock, starvation, oxidative stress, viral infection, hypoxia, UV irradiation that inhibit protein synthesis (Protter and Parker, 2016). Proteomic analysis of the two granules reveals that each has its own distinct but overlapping biomolecular constitution and are organized in the cell by competing multivalent protein interactions (Jain et al., 2016; Kedersha et al., 2005; Wilczynska et al., 2005). Mass spectrometry analysis identified 49 prey proteins that were either associated with PBs and/or SGs **(Figure 16)**. Differential protein interactions between 4E-T WT and 4E-T KR can be divided into the following two groups: First, mass spectrometry revealed a cluster of PB proteins (such as PATL1, EDC3, LSM14A, LSM14B, EIF4E2) that only interacted with 4E-T WT and not 4E-T KR (Group1, see **Table 1**). Second, several PB proteins such as DDX6, CNOT1, IGF2BP1 interacted with both 4E-T WT and 4E-T KR, supporting a multi-step model for PB assembly, wherein 4E-T in its non-ubiquitinated state forms an initial scaffold by interacting with several key PB proteins such as DDX6 (Group 2, see **Table 2**). Monoubiquitination of 4E-T functions as a switch to regulate multivalent interactions with other PB proteins such as LSM14A, PATL1, EDC3, signaling assembly of the entire PB protein interaction network resulting in formation of a functional PB **(Figure 17)**. The inability of 4E-T KR to interact with critical PB components like LSM14A, PATL1, EDC3 amongst others explains the loss of PBs observed with loss of ubiquitination.

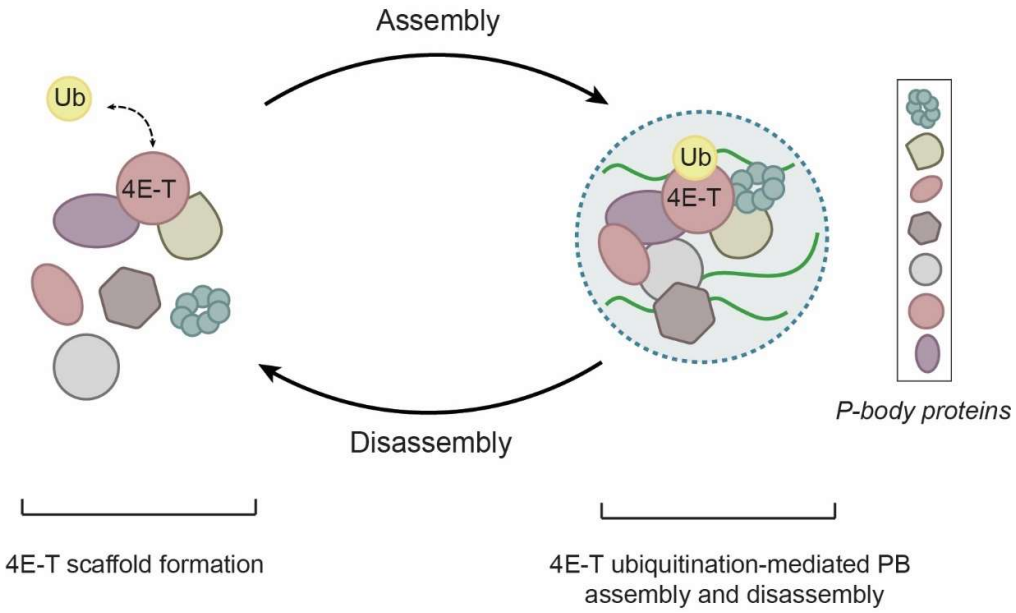

Figure 17. Model depicting 4E-T ubiquitination mediated multi-step assembly of PBs. 4E-T monoubiqutination mediates multi-step assembly of PBs, wherein 4E-T in its non-ubiquitinates state interacts with PB proteins such as DDX6. On ubiquitination, 4E-T can additionally interact with critical PB proteins such as LSM14A and PATL1 to assemble into a functional PB.

5.4.2 Co-immunoprecipitation analysis confirms changes in 4E-T interaction networks.

Mass spectrometry analysis revealed differential 4E-T interaction networks for 4E-T WT and 4E-T KR. To further validate these results, HEK293 cells will first be transfected with either EGFP-4E-T WT or EGFP-4E-T KR and coimmunoprecipitated for 4E-T. The pulled down proteins will be analysed using SDS-PAGE and immunoblotted for LSM14A, IGF2BP1 and PATL1 (Group 1, see Table 1) **(Figure 18)**. Second, HEK293 cells were transfected with

either EGFP-4E-T WT or EGFP-4E-T KR with DDX6-myc (Group 2, see Table 2) and coimmunoprecipitated for 4E-T. The beads were analysed using SDS-PAGE by immunoblotting for Myc **(Figure 19)**.

Similar to mass spectrometry, coimmunoprecipitation revealed a loss of interaction of LSM14A and PATL1 with 4E-T KR. Additionally, as seen on mass spectrometry, an increase in interaction was observed with IGF2BP1 **(Figure 18)**. Furthermore, when HEK293 cells were transfected with DDX6-myc with either 4E-T WT or 4E-T KR, coimmunoprecipitation analysis revealed no change in interaction between 4E-T WT and 4E-T KR, confirming that 4E-T forms an initial scaffold with PB proteins like DDX6 **(Figure 19)**.

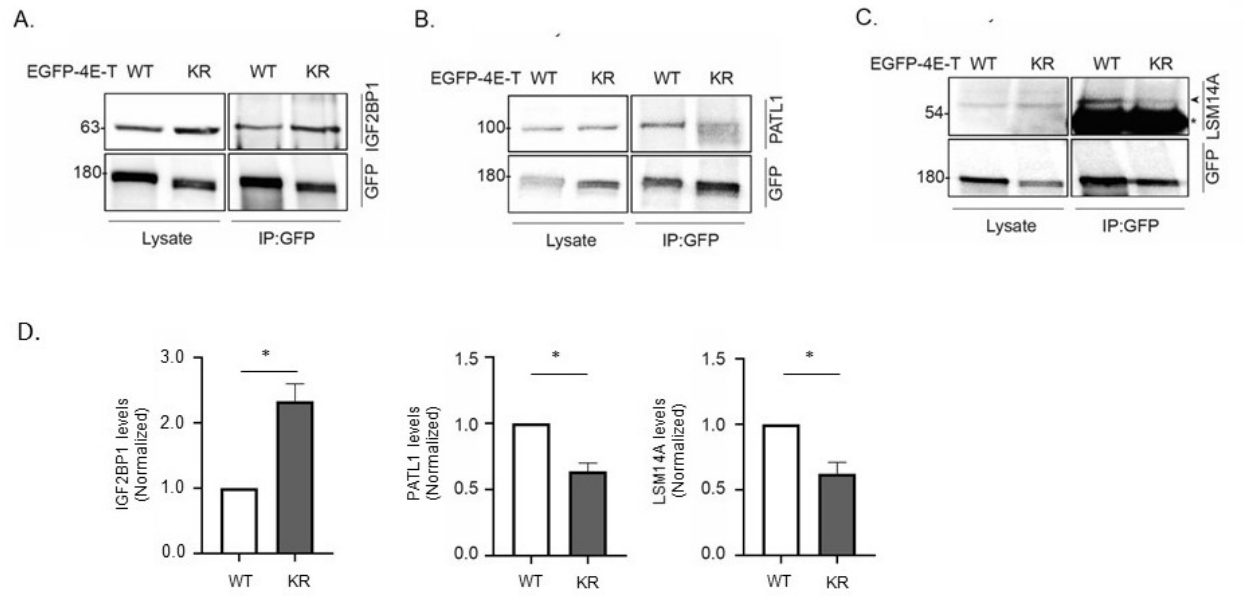

Figure 18. Loss of 4E-T ubiquitination alters 4E-T interaction networks.

Co-immunoprecipitation (with anti-GFP) of HEK293 cells transfected with either EGFP 4E-T WT or EGFP 4E-T KR and immunoblotted for either the target protein or EGFP. (A) Western blot confirmed increased interaction of IGF2BP1 with 4E-T KR compared to 4E-T WT. (B) Western blot analysis confirmed decrease in interaction of PATL1 with 4E-T KR compared to

4E-T WT. (C) Western blot interaction confirmed decrease in interaction of LSM14A with 4E-T KR compared to 4E-T WT. (D) Quantifications depicting relative levels of target protein (IGF2BP1, PATL1 and LSM14A) normalized to 4E-T. Statistical analysis was performed using Student's two-tailed t test. Error bars denote SEM. *p = 0.0376, 0.0299, 0.0499 respectively for n=3 experiments.

Lysate input represents 1.5% of total cell lysate prior to immunoprecipitation. Results are representative of three independent experiments. * indicates IgG heavy chain band. Arrow head indicates target protein band.

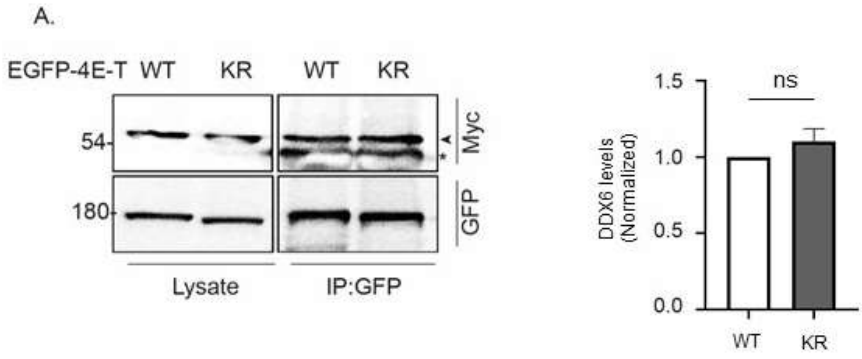

Figure 19. DDX6 interacts equally with 4E-T WT and 4E-T KR.

Co-immunoprecipitation (with anti-GFP) of HEK293 cells transfected with either EGFP 4E-T WT or EGFP 4E-T KR with DDX6-Myc and immunostained with Myc and EGFP. Western blot confirmed that DDX6 interacted equally with EGFP 4E-T WT and EGFP 4E-T KR. Quantifications depicting relative levels of DDX6 normalized to 4E-T. Statistical analysis was

performed using Student's two-tailed t test. Error bars denote SEM. *p = 0.3394 respectively for n=3 experiments.

Lysate input represents 1.5% of total cell lysate prior to immunoprecipitation. Results are representative of three independent experiments. * indicates IgG heavy chain band. Arrow head indicates target protein band.

5.4.3 4E-T ubiquitination mimic (Ub-4E-T) rescues changes in 4E-T interaction networks.

Previous experiments delineated that 4E-T monoubiquitination signals multi-step PB assembly. While essential PB proteins like DDX6 interacted equally with both 4E-T WT and 4E-T KR, several PB proteins like PATL1 interacted only with 4E-T WT, indicating these are part of higher order structures that require 4E-T monoubiquitination. To confirm that changes in 4E-T interaction networks were due to ubiquitination, HEK293 cells were transfected with either V5-4E-T or V5-Ub-4E-T and coimmunoprecipitated for 4E-T using V5 antibody. The pulled down proteins were analysed using SDS-PAGE and immunoblotted for PATL1. The interaction of PB proteins like PATL1 was rescued in presence of Ub-4E-T confirming that the loss of interaction elicited by 4E-T KR was specific to ubiquitination **(Figure 20A)**.

Additionally, to analyse if Ub-4E-T alters 4E-T interaction with scaffolding proteins like DDX6, HEK293 cells were transfected with either V5-4E-T WT or V5-Ub-4E-T and DDX6 and coimmunoprecipitated for 4E-T. The beads were then analysed using SDS-PAGE. Identical interactions between Ub-4E-T and DDX6 was observed, confirming that the ubiquitination mimic does not alter interactions between 4E-T and scaffolding proteins **(Figure 20B)**.

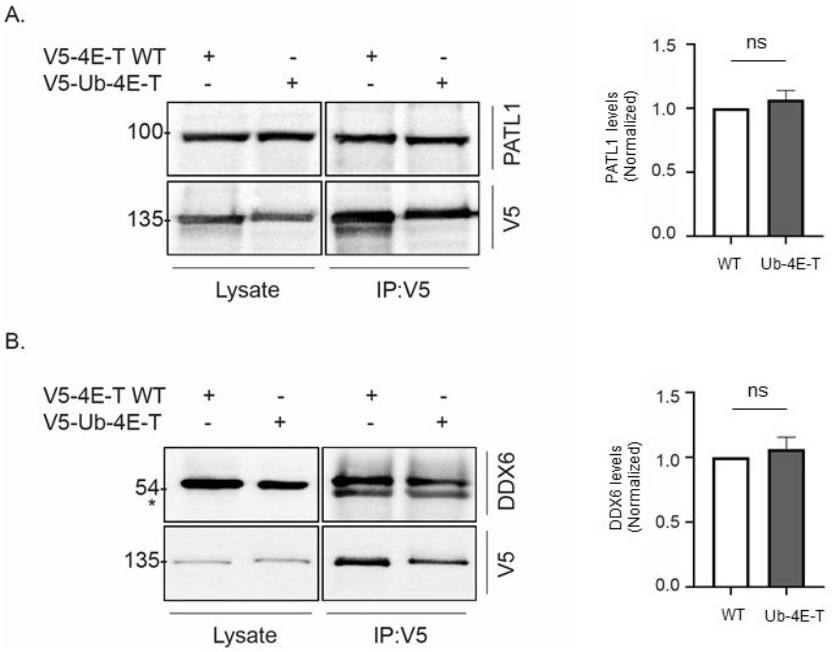

Figure 20. Ub-4E-T (4E-T ubiquitination mimic) rescues changes in 4E-T interaction networks.

Co-immunoprecipitation (with anti-V5) of HEK293 cells transfected with either V5-4E-T WT or V5-Ub-4E-T. (A) Western blot analysis showed PATL1 interacted equally with both 4E-T WT and Ub-4E-T. Quantifications depicting relative levels of PATL1 normalized to 4E-T.

(B) Western blot analysis showed no change in interaction of DDX6 with 4E-T WT and Ub-4E-T. Quantifications depicting relative levels of DDX6 normalized to 4E-T.

Statistical analysis was performed using Student's two-tailed t test. Error bars denote SEM. *p = 0.4324, 0.5605 respectively for n=3 experiments.

Lysate input represents 1.5% of total cell lysate prior to immunoprecipitation. Results are representative of three independent experiments. * indicates IgG heavy chain band.

5.5 Summary

This Chapter confirms that 4E-T ubiquitination drives multi-step PB assembly, wherein non-ubiquitinated 4E-T first assembles a scaffold consisting of core PB proteins like DDX6. Following ubiquitination, 4E-T can further interact with other key PB proteins like LSM14, PATL1 and EDC3 to assemble into a functional PB.

Chapter 6

To determine how the deubiquitinase Otud4 regulates the dynamic monoubiquitination of 4E-T and P-body assembly

Protein ubiquitination is a reversible post-translational modification that alters protein function. Ubiquitination of proteins consists of a three-enzyme cascade wherein, ubiquitin is first activated by ubiquitin activating enzyme (E1) in an ATP-dependent manner, which then binds to the active site of ubiquitin conjugating enzyme (E2). Following this binding, ubiquitin ligase (E3) simultaneously binds to the substrate and E2-Ub intermediate, facilitating the transfer of ubiquitin from E2 to the substrate, resulting in ubiquitination of the substrate (Berndsen and Wolberger, 2014; George et al., 2018; Pickart, 2001). Alternatively, ubiquitin can be removed from the substrate by a class of enzymes called deubiquitinases (DUBs), which further break down the ubiquitin chains to maintain cellular ubiquitin homeostasis (Komander et al., 2009; Mevissen et al., 2013). This bi-directional regulation of ubiquitination facilitates its function as a reversible ON/OFF switch in a myriad of cellular functions (Komander et al., 2009).

Interestingly, liquid-liquid phase separation mediates the dynamic assembly and disassembly of RNP granules such as PBs (Hyman et al., 2014). Previous experiments have delineated that monoubiquitination of 4E-T triggers PB assembly **(Chapter 4 and 5)**. To further dissect out the different components of 4E-T monoubiquitination mediated signaling, it would be critical to identify the DUB regulating PB dynamics, and subsequently assess its role in regulating neural stem cell fate.

Youn et al. conducted a proximity-based mapping study to catalogue PB proteins and their interactors (Youn et al., 2018). The study utilized BioID, a biotin ligase (BirA) was fused

to the bait protein to mediate biotinylation of interacting proteins. Using 4E-T as a bait in HEK293 cells, the study identified Ovarian Tumor Domain Deubiquitinase 4 (Otud4) as a potential deubiquitinase interacting with 4E-T (Youn et al., 2018).

6.1 Otud4 deubiquitinates 4E-T

Youn et al. identified Otud4 as a potential deubiquitnase for 4E-T. To assess if Otud4 deubiquitinates 4E-T, HEK293 cells were transfected with V5-4E-T and HA-Ubiquitin with and without (control) Otud4 overexpression construct. 4E-T was pulled down using V5 antibody and analysed using SDS-PAGE by immunoblotting with V5 (4E-T) and HA (Ubiquitin) **(Figure 21)**. It is expected that if Otud4 deubiquitinates 4E-T a decrease in intensity of ubiquitination band will be observed.

Analysis of ubiquitination band intensity revealed a decrease in 4E-T ubiquitination levels by ~ 50% in HEK293 cells overexpressed with Otud4. Additionally, equal amount of 4E-T was immunoprecipitated between control and cells overexpressing Otud4 **(Figure 21)**.

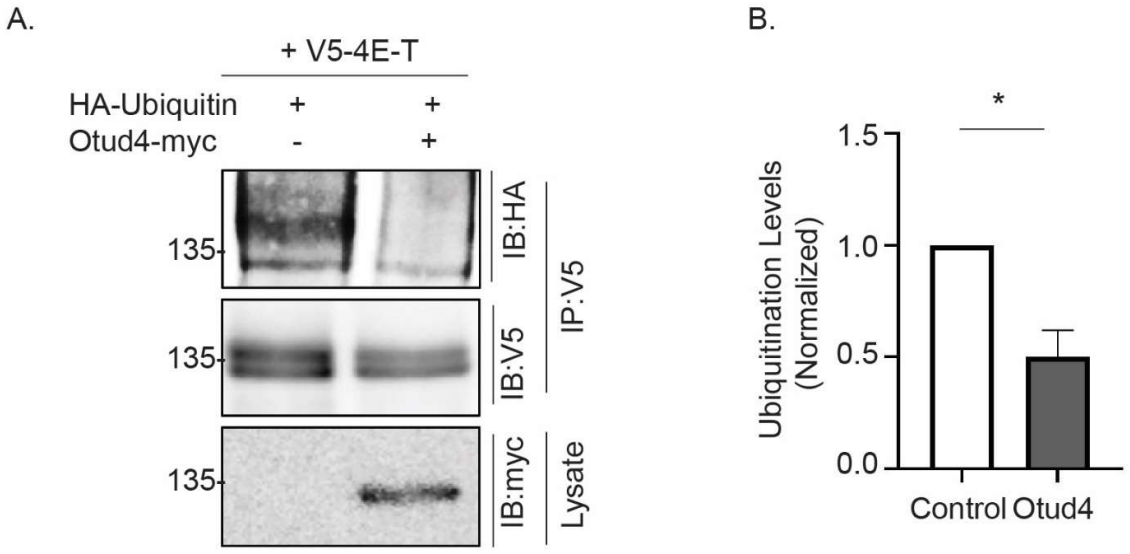

Figure 21. Otud4 deubiquitinates 4E-T.

(A) Immunoprecipitation (with anti-V5) with HEK293 cells transfected with V5-4E-T and HA-Ubiquitin with and without (control) with Otud4-Myc and immunoblotted for Myc and V5. (A) Western blot analysis showed decrease in intensity of ubiquitination band of 4E-T confirming Otud4 deubiquitinates 4E-T. (B) 4E-T ubiquitination bands were normalized to V5-4E-T bands. Quantification of relative 4E-T ubiquitination levels confirmed Otud4 deubiquitinates 4E-T. Statistical analysis was performed using Student's two-tailed t test. Error bars denote SEM. *p=0.01 for n=3 experiments.

Lysate input represents 1.5% of total cell lysate prior to immunoprecipitation. Results are representative of three independent experiments.

6.2 Confirmation of Otud4 interaction with 4E-T

To confirm that Otud4 interacts with 4E-T, HEK293 cells were transfected with Otud4-myc with and without V5-4E-T and reverse coimmunoprecipitated for 4E-T using V5 antibody. The immunoprecipitated products were analysed using western blot and immunoblotted for myc (Otud4) and V5 (4E-T) **(Figure 22).**

Western blot analysis confirmed that coimmunoprecipitation successfully pulled down 4E-T. On immunoblotting for myc, a single band was observed for 4E-T at ~135 kDa, confirming 4E-T interacts with Otud4 **(Figure 22)**.

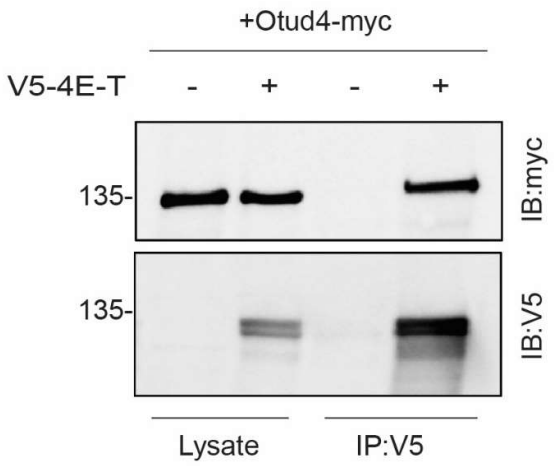

Figure 22. Confirmation of interaction of Otud4 with 4E-T.

Reverse co-immunoprecipitation (with anti-V5) of HEK293 cells transfected with Otud4-myc only and Otud4-myc with V5-4E-T and immunoblotted with V5 and myc. Western blot analysis confirmed interaction of 4E-T with Otud4.

Lysate input represents 1.5% of total cell lysate prior to immunoprecipitation.

6.3 Validation of Otud4 shRNA

To further delineate the effect of Otud4 on PB dynamics, it would be critical to first validate Otud4 shRNA. HEK293 cells were transfected with pEGFP-Otud4 with either shControl or each of the four shOtud4 (1-3). The cell lysates were analysed using SDS-PAGE and probed for EGFP (Otud4) and GAPDH **(Figure 23)**.

The intensity of the EGFP (Otud4) bands was compared for shControl and shOtud4 (1-3). It was found that shOtud4-1 knocked down Otud4 most efficiently with ~75% decrease in Otud4 levels. Therefore, for all further experiments sh-Otud4-1 was used **(Figure 23)**.

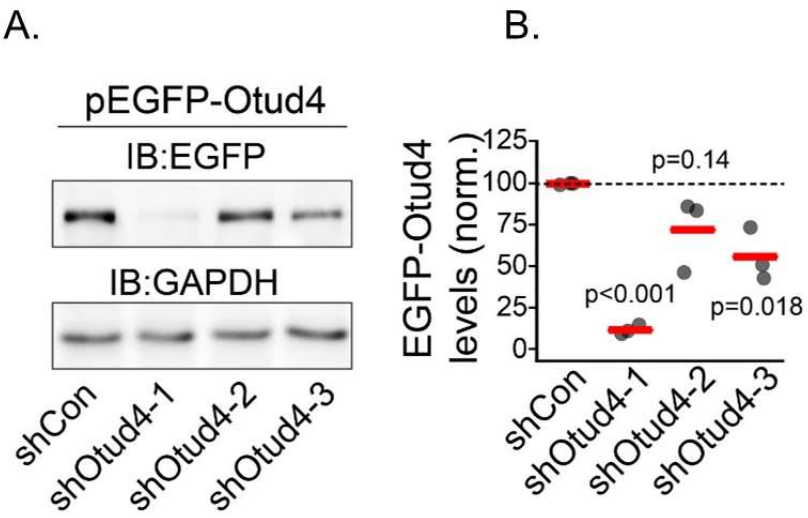

Figure 23. Validation of Otud4 shRNA.

HEK293 cells were transfected with EGFP-Otud4 with shLuciferase (Control) or each of the three shOtud4 (1-3). (A) Western blot analysis (with anti-GFP and anti-Gapdh) and (B) quantification showing change in Otud4 expression relative to Gapdh.

Results are representative of three independent experiments.

6.4 Otud4 regulates PB assembly/disassembly

To study the effects of Otud4 on PBs, E12.5 neural stem cell cultures were transfected with pEGFP only or pEGFP and shOtud4. Neural stem cells were immunostained with PB markers 4E-T and EDC4 and quantified for the number of 4E-T positive foci per cell as well as the number of 4E-T and EDC4 double positive foci **(Figure 24)**. It is expected that if Otud4 deubiquitinates 4E-T, then Otud4 knock down should result in an increase in the number of

PBs. Consistent to this hypothesis, a ~150% in the number of 4E-T positive foci and 4E-T and EDC4 double positive foci per cells **(Figure 24)**.

As a complimentary approach, E12.5 neural stem cell cultures were transfected with pCAGIG (control) or pCAGIG Otud4. Neural stem cells were immunostained with PB markers 4E-T and EDC4 and quantified for the number of 4E-T positive foci and the number of 4E-T and EDC4 double positive foci **(Figure 25)**. It is expected that since Otud4 deubiquitinates 4E-T, overexpression of Otud4 should result in PB disassembly. Consistently, ~40% decrease in number of 4E-T and EDC4 double positive foci, confirming that Otud4 is a critical regulator of PB dynamics **(Figure 25)**.

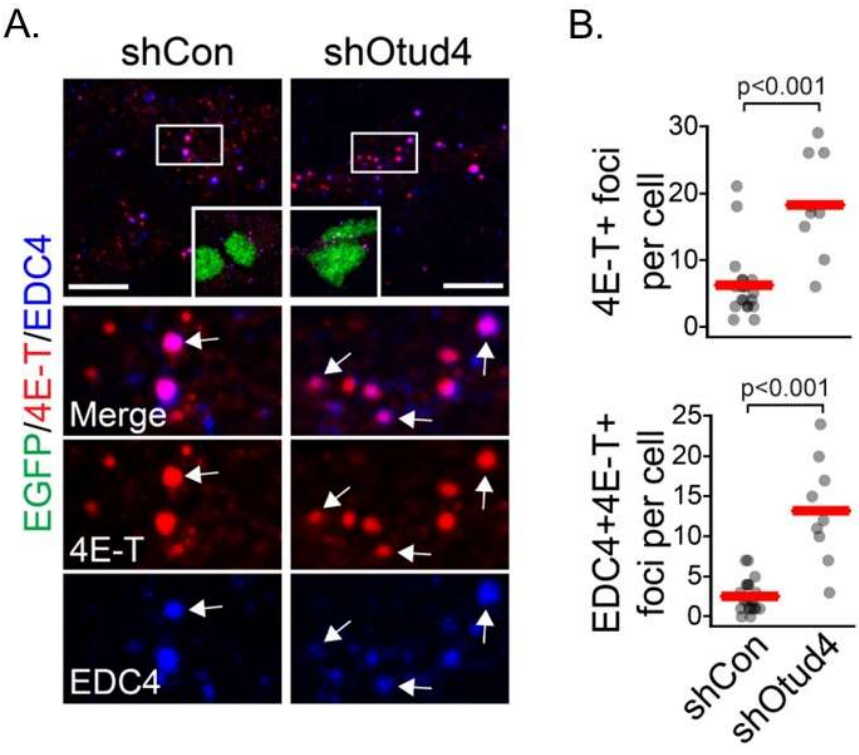

Figure 24. Otud4 knockdown results in increase in PB assembly.

(A) E12.5 neural stem cells were transfected with EGFP and either shLuciferase (control) or shOtud4 and immunostained for EGFP (green), 4E-T (red) and EDC4 (blue). Arrows indicate marker positive foci. Cells were counterstained with Hoechst. (B) Cells were quantified for number of 4E-T positive foci and EDC4 and 4E-T double positive foci. Statistical analysis using Mann-Whitney test. n=20 cells for control and n=10 cells for shOtud4. $p<0.001$, $p<0.001$. Scale bar is 5 μm.

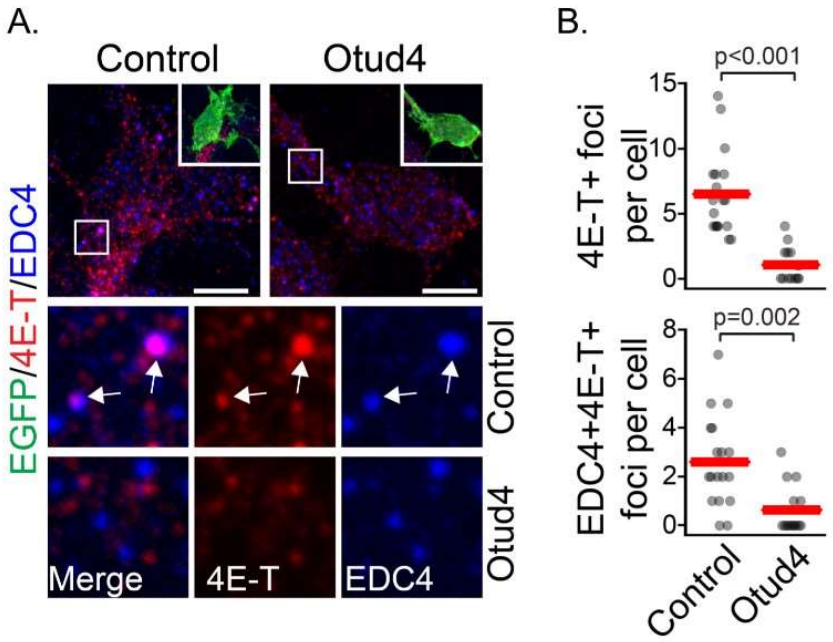

Figure 25. Otud4 overexpression results in PB disassembly.

(A) E12.5 neural stem cells were transfected with either EGFP (control) or EGFP-Otud4 and immunostained for EGFP (green), 4E-T (red) and EDC4 (blue). Arrows indicate marker positive foci. Cells were counterstained with Hoechst. (B) Cells were quantified for number of 4E-T positive foci and EDC4 and 4E-T double positive foci. Each dot represents a cell,

and the crossbar indicates the mean. Statistical analysis using Mann-Whitney test. n=18 cells for control and n=15 cells for Otud4 overexpression. $p<0.001$, $p=0.002$. Scale bar is 5 μm.

6.5 Otud4 mediates PB disassembly through 4E-T deubiquitination

Preliminary analysis in the Yang lab revealed that Otud4 overexpression resulted in PB disassembly. Conversely, knocking down Otud4 increased the number of PBs within the cell. To additionally identify whether this effect of Otud4 on PB assembly/disassembly was mediated through 4E-T ubiquitination or if Otud4 additionally targeted other PB proteins, deubiquitination immunoprecipitation was performed for PB proteins EGFP-CNOT7, DDX6-Myc, EGFP-DCP1a, DCP2-Myc and EGFP-TOP3b. HEK293 cells were transfected with each of the target proteins alone, with HA-Ubiquitin with and without (control) Otud4-Myc **(Figure 26)**. Similar to the approach used before, the target protein was immunoprecipitated and the beads were analysed using western blot by immunoblotting for the target protein and HA (ubiquitin).

Western blot analysis revealed that an equal amount of target protein was pulled down between control and Otud4 overexpressing cells. No change in intensity of ubiquitination bands was observed for each target protein, confirming that Otud4 specifically deubiquitinates 4E-T to regulate PB dynamics **(Figure 26)**.

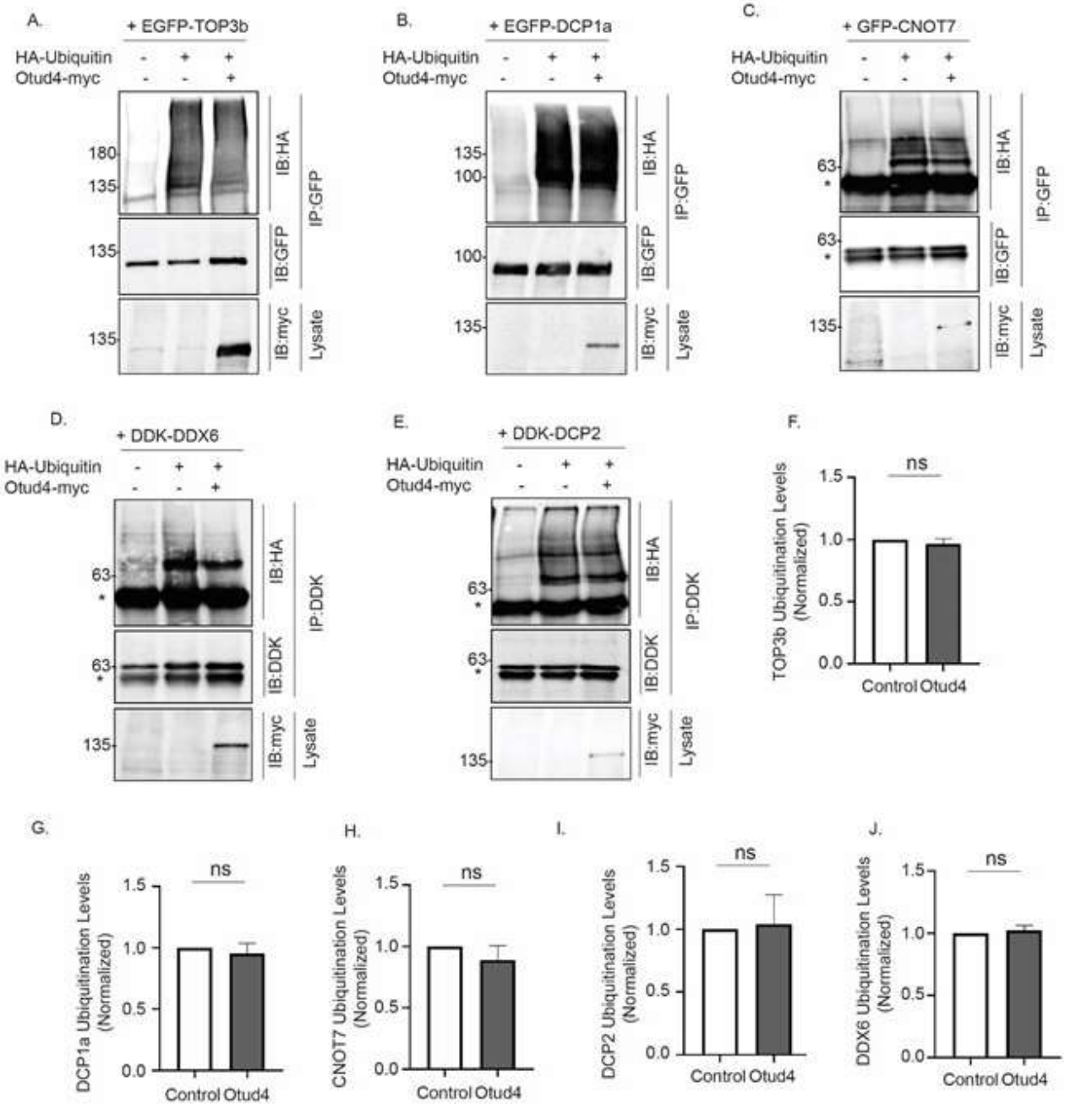
A.
+ EGFP-TOP3b
HA-Ubiquitin - + +
Otud4-myc - - +
180
135
135
135
IB:HA
IB:GFP
IB:myc
IP:GFP
Lysate
B.
+ EGFP-DCP1a
HA-Ubiquitin - + +
Otud4-myc - - +
135
100
100
135
IB:HA
IB:GFP
IB:myc
IP:GFP
Lysate
C.
+ GFP-CNOT7
HA-Ubiquitin - + +
Otud4-myc - - +
63
*
63
*
135
IB:HA
IB:GFP
IB:myc
IP:GFP
Lysate
D.
+ DDK-DDX6
HA-Ubiquitin - + +
Otud4-myc - - +
63
*
63
*
135
IB:HA
IB:DDK
IB:myc
IP:DDK
Lysate
E.
+ DDK-DCP2
HA-Ubiquitin - + +
Otud4-myc - - +
63
*
63
*
135
IB:HA
IB:DDK
IB:myc
IP:DDK
Lysate
F.
TOP3b Ubiquitination Levels (Normalized)
ns
1.5
1.0
0.5
0.0
Control Otud4
G.
DCP1a Ubiquitination Levels (Normalized)
ns
1.5
1.0
0.5
0.0
Control Otud4
H.
CNOT7 Ubiquitination Levels (Normalized)
ns
1.5
1.0
0.5
0.0
Control Otud4
I.
DCP2 Ubiquitination Levels (Normalized)
ns
1.5
1.0
0.5
0.0
Control Otud4
J.
DDX6 Ubiquitination Levels (Normalized)
ns
1.5
1.0
0.5
0.0
Control Otud4

Figure 26. Otud4 does not deubiquitinate other core PB proteins.

Ubiquitination assay of HEK293 cells transfected with epitope tagged target protein and HA-Ubiquitin with or without (control) Otud4. Western blot analysis showing no change in ubiquitination levels for (A) EGFP-Top3b, (B) EGFP-DCP1a, (C) EGFP-CNOT7, (D) DDK-DDX6 and (E) DDK-DCP2 between control and cells transfected with Otud4. (F-J) Ubiquitination bands were normalized to target protein levels. Quantification of relative ubiquitination levels confirm that Otud4 does not deubiquitinate other core PB proteins. Statistical analysis was performed using Student's two-tailed t test. Error bars denote SEM. p = 0.66, p= 0.59, p=0.39, p=0.59, p=0.87 for n=3 experiments.

Lysate input represents 1.5% of total cell lysate prior to immunoprecipitation. Results are representative of three independent experiments. * indicates IgG heavy chain band.

6.6 Otud4 regulates 4E-T ubiquitination through its catalytic activity.

Otud4 contains the ovarian tumor domain and therefore, belongs to the subfamily of OTU deubiquitinases. It has been implicated in a myriad of biological processes such as anti-viral immune response, innate immunity as well as osmoregulation (Liuyu et al., 2019; Tse et al., 2013; Zhao et al., 2015). Additionally, previous literature has identified that Otud4 regulates protein activity by functioning as a scaffold to bind other deubiquitinases such as USP9X and USP11 (Zhao et al., 2015). This non-catalytic function of Otud4 raises the question, if Otud4 specifically deubiquitinates 4E-T or alternatively, facilitates indirect interaction with other deubiquitinases.

To address this question, a catalytically inactive form of Otud4 (Otud4-Δ), lacking the catalytic domain at N-terminus was used. It is expected that in absence of the catalytic domain, Otud4-Δ lacks its deubiquitination activity. HEK293 cells were transfected with V5-4E-T, HA-

Ubiquitin (control). Alternatively, HEK293 cells were transfected with V5-4E-T, HA-Ubiquitin and Otud4-Δ. 4E-T was immunoprecipitated using V5 antibody and analysed by SDS-PAGE by immunoblotting for V5 (4E-T) and HA (Ubiquitin).

Western blot analysis revealed no change in 4E-T ubiquitination band intensity between control and HEK293 cells overexpressed with Otud4-Δ, suggesting that the deubiquitination of 4E-T observed is dependent on its catalytic activity **(Figure 27)**.

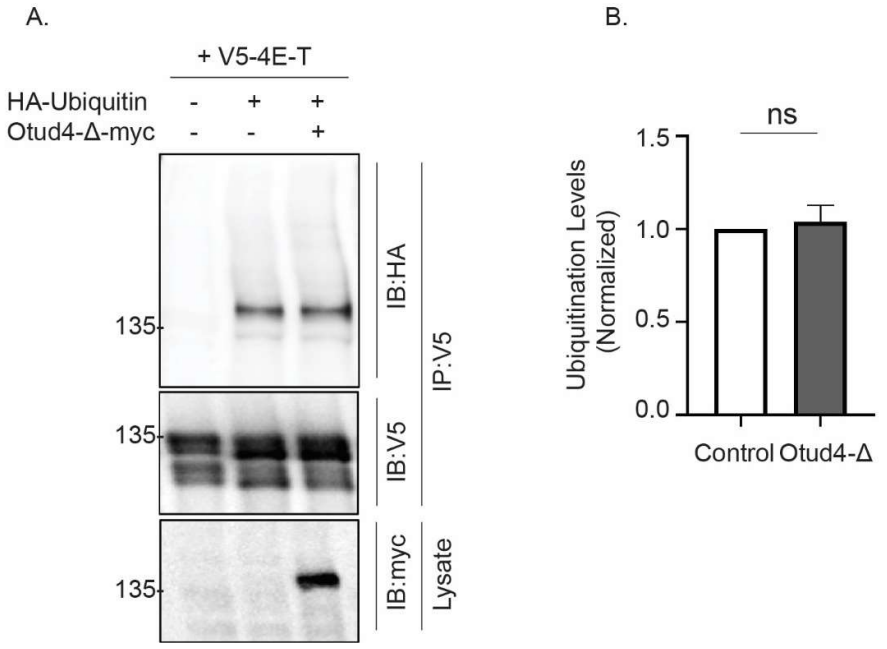

Figure 27. Otud4 deubiquitinates 4E-T through its catalytic activity.

(A) Immunoprecipitation (with anti-V5) of HEK293 cells transfected with V5-4E-T only, V5-4E-T and HA-Ubiquitin with and without (control) with Otud4-Δ (deletion of catalytic domain at N-terminus) and immunoblotted with HA (ubiquitin) and V5 (4E-T). Western blot analysis confirmed no change in 4E-T ubiquitination levels in control and cells transfected with Otud4-Δ. (B) 4E-T ubiquitination levels were normalized to V5-4E-T. Quantification of relative 4E-

T ubiquitination levels confirm Otud4 deubiquitinates 4E-T depending on its catalytic activity. Statistical analysis was performed using Student's two-tailed t test. Error bars denote SEM. p = 0.66 for n=3 experiments.

Lysate input represents 1.5% of total cell lysate prior to immunoprecipitation. Results are representative of three independent experiments.

6.7 Summary

This Chapter confirms that Otud4 mediated deubiquitination of 4E-T regulates PB dynamics, wherein Otud4 overexpression resulted in a loss of PBs. On the other end, Otud4 knock-down using shRNA result in a corresponding increase in the number of PBs.

Chapter 7

Discussion

Membrane-less RNP granules such as PBs maintain stem cell homeostasis by regulating eukaryotic gene expression, wherein they serve as temporary mRNA reservoirs to supress mRNA translation. To delineate how PB dynamics regulate neural stem cell fate, it would be important to understand the molecular signaling regulating PB assembly/disassembly. Recently, protein ubiquitination has emerged as an important post-translational modification regulating LLPS (Dao et al., 2018; Gallego et al., 2020; Yasuda et al., 2020). For instance, liquid-liquid phase separated pathological aggregates in neurodegenerative disorders like frontotemporal dementia (FTD) and amyotrophic lateral sclerosis (ALS) were found enriched in ubiquitinated TDP-43 (Neumann et al., 2006). Therefore, understanding the molecular signaling regulating assembly of RNP granules such as PBs would help characterize their role in normal and diseased conditions.

Here, I found that 4E-T, a core PB protein is monoubiquitinated and this ubiquitination drives PB assembly. This result is particularly intriguing because first, 4E-T is critical for PB assembly and second, it regulates neural stem cell maintenance. Additionally, non-proteolytic monoubiquitination often serves signaling functions in the cell.

One interesting question regarding this model is how 4E-T monoubiquitination drives rapid and accurate assembly of PBs. Recent research has shown that these biomolecular condensates contain scaffolds, proteins that drive PB assembly as well as clients which bind to scaffold to phase separate into these condensates (Alberti et al., 2019). Our data shows that 4E-T prior to ubiquitination forms a scaffold with key PB proteins like DDX6. Monoubiquitination of 4E-T signals formation of multivalent interactions with other PB proteins like LSM14A, EDC3, EIF4E2, assembling a functional PB **(Figure 22)**. 4E-T KR forms the initial scaffold

locking in and exhausting the available scaffolding proteins, preventing assembly of endogenous PBs. This multi-step PB assembly explains the dominant negative effect of 4E-T KR on PB formation.

PBs sequester mRNA away from translation machinery and function as transient mRNA storage sites (Brengues et al., 2005; Luo et al., 2018). Previous research has delineated that specific RNA-protein interactions between RNA-binding proteins such as IGF2BP1, PUM2, MOV10 and their respective mRNA targets regulate segregation of mRNA into PBs (Hubstenberger et al., 2017; Wang et al., 2018). The multistep assembly of PBs around scaffold proteins regulated by 4E-T monoubiquitination offers several advantages. First, PB assembly around scaffold proteins and the tuneable segregation of more customised RNA-binding client proteins with their specific mRNA targets explains the target specific heterogeneity in the molecular constitution of PBs. This customization explains that while PBs are ubiquitously present across different cell types during mammalian brain development, depending on the mRNA repertoire, there exists variability in the biological effects they elicit. For instance, PBs have previously been shown to be important regulators of neurogenesis by repressing translation of pro-neurogenic mRNAs facilitating maintenance of neural stem cell fate (Amadei et al., 2015; Yang et al., 2014). Additionally, during neurogenesis PBs define cortical neuronal identity by differentially targeting deep vs superficial layer specific mRNAs (Zahr et al., 2018). Second, this multistep assembly allows for formation of a standardized stable scaffold, which provides a structural platform to partition different client proteins, facilitating rapid turnover of PBs (Wheeler et al., 2016). This dynamic assembly and disassembly can allow PBs to rapidly fine-tune the untranslated mRNA pool regulating neural stem cell fate decisions.

What intrinsic signals regulate 4E-T ubiquitination to fine-tune PB assembly? The dynamic regulation of monoubiquitination by E3 ligases and deubiquitinases allows ubiquitination to function as a reversible ON/OFF switch regulating a variety of cellular

functions. Here, we found that Otud4 regulates 4E-T ubiquitination to modulate PB dynamics. Otud4 overexpression in E12.5 neural stem cell cultures phenocopies the results obtained with 4E-T KR confirming that loss of monoubiquitination of 4E-T inhibits PB assembly. On the other end, Otud4 knock down resulted in an increase in the number of PBs. Intriguingly, this Otud4 deubiquitination action was highly specific and no change in ubiquitination levels was observed for other PB proteins such as DCP1a, DCP2, CNOT7, DDX6 and TOP3b. These results provide novel insights into a non-proteolytic ubiquitination mechanism regulating PBs.

The role of deubiquitinases and non-proteolytic ubiquitination in regulating cortical development still remains largely unknown. Interestingly, Otud4 mutation has been linked to a rare neurodevelopmental syndrome of hypogonadotropic hypogonadism, ataxia and dementia (Margolin et al., 2013). Previous research has shown that perturbations of proper PB regulation can affect cortical development (Lennox et al., 2020; Yang et al., 2014; Zahr et al., 2018). Therefore, addressing the role of Otud4 in regulating PBs will be important to further address the role of Otud4 on cortical development as well to understand how RNP granules like PBs determine proper cortical development.

Chapter 8

Future directions

This project delineated a non-proteolytic ubiquitination-based signaling mechanism regulating PB dynamics, wherein reversible ubiquitination of 4E-T regulated by deubiquitinase Otud4 drives PB assembly/disassembly. Research in the Yang lab has explored the implication of this ubiquitination based PB assembly on neural stem cell fate. Preliminary data suggests that PBs are critical regulators of neural stem cell homeostasis and PB disassembly can drive neural stem cell differentiation into neurons. To this end, PB disassembly mediated by Otud4 overexpression promoted neural stem cell differentiation. Alternatively, PB assembly regulated by Otud4 knock down resulted in neural stem cell fate maintenance.

8.1 Identifying the monoubiquitination site for 4E-T

To additionally confirm the effects of 4E-T monoubiquitination on PB dynamics, it would be critical to identify the monoubiquitination site of 4E-T. To identify the ubiquitination site mass spectrometry will be performed for V5-4E-T WT and V5-4E-T WT treated with 1 μM TAK 243 for four hours. Additionally, this approach will be supplemented by creating different 4E-T mutants, wherein different range of lysines in the protein will be mutated to arginines. To this end, the ubiquitination status of these mutants will be assessed using immunoprecipitation and SDS-PAGE.

8.2 Identifying the E3 Ligase ubiquitinating 4E-T

The bi-directional regulation of ubiquitination by E3 ubiquitin ligases and deubiquitinases allows ubiquitination to function as a reversible ON/OFF switch to regulate

cellular function. Therefore, to delineate the molecular mechanism of 4E-T ubiquitination mediated PB assembly, it would be critical to identify the E3 ligase ubiquitinating 4E-T. Youn et al. conducted a proximity-based mapping study to catalogue PB proteins and their interactors (Youn et al., 2018). Using 4E-T as a bait in HEK293 cells, the study identified E3 ligases and adaptor proteins DDB1 and CUL4 Associated Factor 7 (Dcaf7), Roquin 1 (Rc3h1), Ring Finger Protein 214 (Rnf214) and Tripartite Motif Containing 56 (Trim56) to possibly mediate 4E-T monoubiquitination (Youn et al., 2018). The next step will be to identify the E3 ligase ubiquitinating 4E-T. HEK293 cells will be transfected with V5-4E-T and HA-Ubiquitin and with and without (control) an overexpression construct for each of the four E3 ligases and immunoprecipitated for 4E-T (V5). It is expected that overexpression of the E3 ligase should result in a corresponding increase in 4E-T ubiquitination. Preliminary experiments in the Yang lab suggest that Trim56 ubiquitinates 4E-T.

Additionally, to better understand how Trim56 regulates PB dynamics, overexpression and knock down experiments will be performed and corresponding changes in PB numbers will be assessed.

8.3 Examination of mRNA translational profile in neural stem cells during embryonic development

Previous studies have implicated that PBs can function as temporary mRNA storage reservoirs to sequester mRNAs away from the translational machinery, inhibiting their translation. This repression is temporary and PB disassembly can release mRNA back to the cytosol for translation. To mechanistically understand the effects of PB dynamics on neural stem cell homeostasis, it would therefore be critical assess changes in the translational status of mRNAs.

Polysome profiling offers a powerful tool to assess the translational status of mRNAs, wherein free/ poorly translated mRNAs (associated with monosomes) can be separated from highly translated mRNAs (associated with polysomes) using a sucrose density gradient. To understand how PB assembly/disassembly will alter mRNA translation rates in neural stem cells, polysome profiling will be performed for controls (*CreER, Otud4* $^{+/+}$) and conditional Otud4 knock out mice (*CreER, Otud4*$^{fl/fl}$) at embryonic day 12.5, since at this stage the majority of cells in the cortex are neural stem cells. Broadly, cortical tissue will first be lysed, and the tissue lysates will be loaded on a sucrose density gradient. This gradient will then be ultracentrifuged and the fractions will be analysed and collected. RNA will be extracted from these fractions and analysed using RNA-sequencing. The differences in mRNA association with low translated monosomes and heavier translated polysomes will help ascertain the mRNA translation status.

Chapter 9

Conclusion

Proper development of complex organ systems such as the mammalian brain relies on a delicate balance between stem cell self-renewal and its differentiation into different cell types. During cortical development 4E-T plays a critical role in stem cell fate maintenance by sequestering specific mRNAs in PBs and suppressing their translation. Disruptions in this process can result in neurodevelopmental disorders such as Autism Spectrum Disorder and schizophrenia. Thus, understanding the molecular mechanism behind P-body assembly will not only give us useful insights about the translational regulation of gene expression, but will also be important in understanding how dynamic organelles like P-bodies mediate the formation of complex organ systems like the human brain.

The project delineated a non-proteolytic ubiquitination-based mechanism regulating PB dynamics, wherein dynamic monoubiquitination of 4E-T regulated by deubiquitinase Otud4 drives PB assembly **(Figure 17)**. The project provides novel insights into understanding the molecular signaling mechanism regulating PB assembly/disassembly and can be used as a tool to further address how PB dynamics can regulate stem cell homeostasis.

References

Akutsu, M., Dikic, I., and Bremm, A. (2016). Ubiquitin chain diversity at a glance. J. Cell Sci. *129*, 875–880.

Alberti, S., Gladfelter, A., and Mittag, T. (2019). Considerations and Challenges in Studying Liquid-Liquid Phase Separation and Biomolecular Condensates. Cell *176*, 419–434.

Amadei, G., Zander, M.A., Yang, G., Dumelie, J.G., Vessey, J.P., Lipshitz, H.D., Smibert, C.A., Kaplan, D.R., and Miller, F.D. (2015). A Smaug2-Based Translational Repression Complex Determines the Balance between Precursor Maintenance versus Differentiation during Mammalian Neurogenesis. J. Neurosci. *35*, 15666–15681.

Bah, A., and Forman-Kay, J.D. (2016). Modulation of Intrinsically Disordered Protein Function by Post-translational Modifications. J. Biol. Chem. *291*, 6696–6705.

Banani, S.F., Rice, A.M., Peeples, W.B., Lin, Y., Jain, S., Parker, R., and Rosen, M.K. (2016). Compositional Control of Phase-Separated Cellular Bodies. Cell *166*, 651–663.

Berndsen, C.E., and Wolberger, C. (2014). New insights into ubiquitin E3 ligase mechanism. Nat. Struct. Mol. Biol. *21*, 301–307.

Boeynaems, S., Alberti, S., Fawzi, N.L., Mittag, T., Polymenidou, M., Rousseau, F., Schymkowitz, J., Shorter, J., Wolozin, B., Van Den Bosch, L., et al. (2018). Protein Phase Separation: A New Phase in Cell Biology. Trends Cell Biol. *28*, 420–435.

Brengues, M., Teixeira, D., and Parker, R. (2005). Movement of Eukaryotic mRNAs Between Polysomes and Cytoplasmic Processing Bodies. Science *310*, 486–489.

Custo Greig, L., Woodworth, M., Galazo, M., Padmanabhan, H., and Macklis, J. (2013a). Molecular logic of neocortical projection neuron specification, development and diversity. Nat. Rev. Neurosci. *14*.

Custo Greig, L., Woodworth, M., Galazo, M., Padmanabhan, H., and Macklis, J. (2013b). Molecular logic of neocortical projection neuron specification, development and diversity. Nat. Rev. Neurosci. *14*.

Dao, T.P., Kolaitis, R.-M., Kim, H.J., O'Donovan, K., Martyniak, B., Colicino, E., Hehnly, H., Taylor, J.P., and Castañeda, C.A. (2018). Ubiquitin Modulates Liquid-Liquid Phase Separation of UBQLN2 via Disruption of Multivalent Interactions. Mol. Cell *69*, 965-978.e6.

Deribe, Y.L., Pawson, T., and Dikic, I. (2010). Post-translational modifications in signal integration. Nat. Struct. Mol. Biol. *17*, 666–672.

Diekmann, Y., and Pereira-Leal, J.B. (2012). Evolution of intracellular compartmentalization. Biochem. J. *449*, 319–331.

Durak, O., Gao, F., Kaeser-Woo, Y.J., Rueda, R., Martorell, A.J., Nott, A., Liu, C.Y., Watson, L.A., and Tsai, L.-H. (2016). Chd8 mediates cortical neurogenesis via transcriptional regulation of cell cycle and Wnt signaling. Nat. Neurosci. *19*, 1477–1488.

Eulalio, A., Behm-Ansmant, I., and Izaurralde, E. (2007a). P bodies: at the crossroads of post-transcriptional pathways. Nat. Rev. Mol. Cell Biol. *8*, 9–22.

Eulalio, A., Behm-Ansmant, I., Schweizer, D., and Izaurralde, E. (2007b). P-body formation is a consequence, not the cause, of RNA-mediated gene silencing. Mol. Cell. Biol. *27*, 3970–3981.

Fernandopulle, M.S., Lippincott-Schwartz, J., and Ward, M.E. (2021). RNA transport and local translation in neurodevelopmental and neurodegenerative disease. Nat. Neurosci. 1–11.

Ford, L., Ling, E., Kandel, E.R., and Fioriti, L. (2019). CPEB3 inhibits translation of mRNA targets by localizing them to P bodies. Proc. Natl. Acad. Sci. *116*, 18078–18087.

Gabaldón, T., and Pittis, A.A. (2015). Origin and evolution of metabolic sub-cellular compartmentalization in eukaryotes. Biochimie *119*, 262–268.

Gallego, L.D., Schneider, M., Mittal, C., Romanauska, A., Gudino Carrillo, R.M., Schubert, T., Pugh, B.F., and Köhler, A. (2020). Phase separation directs ubiquitination of gene-body nucleosomes. Nature *579*, 592–597.

George, A.J., Hoffiz, Y.C., Charles, A.J., Zhu, Y., and Mabb, A.M. (2018). A Comprehensive Atlas of E3 Ubiquitin Ligase Mutations in Neurological Disorders. Front. Genet. *9*.

Gkogkas, C.G., Khoutorsky, A., Ran, I., Rampakakis, E., Nevarko, T., Weatherill, D.B., Vasuta, C., Yee, S., Truitt, M., Dallaire, P., et al. (2013). Autism-related deficits via dysregulated eIF4E-dependent translational control. Nature *493*, 371–377.

Gomes, E., and Shorter, J. (2019). The molecular language of membraneless organelles. J. Biol. Chem. *294*, 7115–7127.

Götz, M., and Huttner, W.B. (2005). The cell biology of neurogenesis. Nat. Rev. Mol. Cell Biol. *6*, 777–788.

Guillén-Boixet, J., Kopach, A., Holehouse, A.S., Wittmann, S., Jahnel, M., Schlüßler, R., Kim, K., Trussina, I.R.E.A., Wang, J., Mateju, D., et al. (2020). RNA-Induced Conformational Switching and Clustering of G3BP Drive Stress Granule Assembly by Condensation. Cell *181*, 346-361.e17.

Hall, P.A., and Watt, F.M. (1989). Stem cells: the generation and maintenance of cellular diversity. Dev. Camb. Engl. *106*, 619–633.

Heins, N., Malatesta, P., Cecconi, F., Nakafuku, M., Tucker, K.L., Hack, M.A., Chapouton, P., Barde, Y.-A., and Götz, M. (2002). Glial cells generate neurons: the role of the transcription factor Pax6. Nat. Neurosci. *5*, 308–315.

Herhaus, L., and Dikic, I. (2015). Expanding the ubiquitin code through post-translational modification. EMBO Rep. *16*, 1071–1083.

Hubstenberger, A., Courel, M., Bénard, M., Souquere, S., Ernoult-Lange, M., Chouaib, R., Yi, Z., Morlot, J.-B., Munier, A., Fradet, M., et al. (2017). P-Body Purification Reveals the Condensation of Repressed mRNA Regulons. Mol. Cell *68*, 144-157.e5.

Hyer, M.L., Milhollen, M.A., Ciavarri, J., Fleming, P., Traore, T., Sappal, D., Huck, J., Shi, J., Gavin, J., Brownell, J., et al. (2018). A small-molecule inhibitor of the ubiquitin activating enzyme for cancer treatment. Nat. Med. *24*, 186–193.

Hyman, A.A., Weber, C.A., and Jülicher, F. (2014). Liquid-Liquid Phase Separation in Biology. Annu. Rev. Cell Dev. Biol. *30*, 39–58.

Imayoshi, I., and Kageyama, R. (2014). bHLH Factors in Self-Renewal, Multipotency, and Fate Choice of Neural Progenitor Cells. Neuron *82*, 9–23.

Iwata, R., Casimir, P., and Vanderhaeghen, P. (2020). Mitochondrial dynamics in postmitotic cells regulate neurogenesis. Science *369*, 858–862.

Jain, S., Wheeler, J.R., Walters, R.W., Agrawal, A., Barsic, A., and Parker, R. (2016). ATPase-Modulated Stress Granules Contain a Diverse Proteome and Substructure. Cell *164*, 487–498.

Kedersha, N., Stoecklin, G., Ayodele, M., Yacono, P., Lykke-Andersen, J., Fritzler, M.J., Scheuner, D., Kaufman, R.J., Golan, D.E., and Anderson, P. (2005). Stress granules and processing bodies are dynamically linked sites of mRNP remodeling. J. Cell Biol. *169*, 871–884.

Khacho, M., Clark, A., Svoboda, D.S., Azzi, J., MacLaurin, J.G., Meghaizel, C., Sesaki, H., Lagace, D.C., Germain, M., Harper, M.-E., et al. (2016). Mitochondrial Dynamics Impacts Stem Cell Identity and Fate Decisions by Regulating a Nuclear Transcriptional Program. Cell Stem Cell *19*, 232–247.

Kim, J.Y., Liu, C.Y., Zhang, F., Duan, X., Wen, Z., Song, J., Feighery, E., Lu, B., Rujescu, D., St Clair, D., et al. (2012). Interplay between DISC1 and GABA Signaling Regulates Neurogenesis in Mice and Risk for Schizophrenia. Cell *148*, 1051–1064.

Komander, D., Clague, M.J., and Urbé, S. (2009). Breaking the chains: structure and function of the deubiquitinases. Nat. Rev. Mol. Cell Biol. *10*, 550–563.

Kriegstein, A., and Alvarez-Buylla, A. (2009). The Glial Nature of Embryonic and Adult Neural Stem Cells. Annu. Rev. Neurosci. *32*, 149–184.

Lennox, A.L., Hoye, M.L., Jiang, R., Johnson-Kerner, B.L., Suit, L.A., Venkataramanan, S., Sheehan, C.J., Alsina, F.C., Fregeau, B., Aldinger, K.A., et al. (2020). Pathogenic DDX3X Mutations Impair RNA Metabolism and Neurogenesis during Fetal Cortical Development. Neuron *106*, 404-420.e8.

Liuyu, T., Yu, K., Ye, L., Zhang, Z., Zhang, M., Ren, Y., Cai, Z., Zhu, Q., Lin, D., and Zhong, B. (2019). Induction of OTUD4 by viral infection promotes antiviral responses through deubiquitinating and stabilizing MAVS. Cell Res. *29*, 67–79.

Lui, J., Castelli, L.M., Pizzinga, M., Simpson, C.E., Hoyle, N.P., Bailey, K.L., Campbell, S.G., and Ashe, M.P. (2014). Granules Harboring Translationally Active mRNAs Provide a Platform for P-Body Formation following Stress. Cell Rep. *9*, 944–954.

Luo, Y., Na, Z., and Slavoff, S.A. (2018). P-Bodies: Composition, Properties, and Functions. Biochemistry *57*, 2424–2431.

Margolin, D.H., Kousi, M., Chan, Y.-M., Lim, E.T., Schmahmann, J.D., Hadjivassiliou, M., Hall, J.E., Adam, I., Dwyer, A., Plummer, L., et al. (2013). Ataxia, dementia, and hypogonadotropism caused by disordered ubiquitination. N. Engl. J. Med. *368*, 1992–2003.

Markmiller, S., Fulzele, A., Higgins, R., Leonard, M., Yeo, G.W., and Bennett, E.J. (2019). Active Protein Neddylation or Ubiquitylation Is Dispensable for Stress Granule Dynamics. Cell Rep. *27*, 1356-1363.e3.

Martynoga, B., Drechsel, D., and Guillemot, F. (2012). Molecular Control of Neurogenesis: A View from the Mammalian Cerebral Cortex. Cold Spring Harb. Perspect. Biol. *4*.

Mason, A.F., Yewdall, N.A., Welzen, P.L.W., Shao, J., van Stevendaal, M., van Hest, J.C.M., Williams, D.S., and Abdelmohsen, L.K.E.A. (2019). Mimicking Cellular Compartmentalization in a Hierarchical Protocell through Spontaneous Spatial Organization. ACS Cent. Sci. *5*, 1360–1365.

Mevissen, T.E.T., Hospenthal, M.K., Geurink, P.P., Elliott, P.R., Akutsu, M., Arnaudo, N., Ekkebus, R., Kulathu, Y., Wauer, T., El Oualid, F., et al. (2013). OTU Deubiquitinases Reveal Mechanisms of Linkage Specificity and Enable Ubiquitin Chain Restriction Analysis. Cell *154*, 169–184.

Mitrea, D.M., Cika, J.A., Stanley, C.B., Nourse, A., Onuchic, P.L., Banerjee, P.R., Phillips, A.H., Park, C.-G., Deniz, A.A., and Kriwacki, R.W. (2018). Self-interaction of NPM1 modulates multiple mechanisms of liquid–liquid phase separation. Nat. Commun. *9*, 842.

Moriwaki, K., and Chan, F.K.-M. (2016). Regulation of RIPK3- and RHIM-dependent Necroptosis by the Proteasome. J. Biol. Chem. *291*, 5948–5959.

Muroyama, Y., Fujiwara, Y., Orkin, S.H., and Rowitch, D.H. (2005). Specification of astrocytes by bHLH protein SCL in a restricted region of the neural tube. Nature *438*, 360–363.

Neumann, M., Sampathu, D.M., Kwong, L.K., Truax, A.C., Micsenyi, M.C., Chou, T.T., Bruce, J., Schuck, T., Grossman, M., Clark, C.M., et al. (2006). Ubiquitinated TDP-43 in Frontotemporal Lobar Degeneration and Amyotrophic Lateral Sclerosis. Science *314*, 130–133.

Nicklas, S., Hillje, A.-L., Okawa, S., Rudolph, I.-M., Collmann, F.M., van Wuellen, T., Del Sol, A., and Schwamborn, J.C. (2019). A complex of the ubiquitin ligase TRIM32 and the deubiquitinase USP7 balances the level of c-Myc ubiquitination and thereby determines neural stem cell fate specification. Cell Death Differ. *26*, 728–740.

Noctor, S.C., Flint, A.C., Weissman, T.A., Dammerman, R.S., and Kriegstein, A.R. (2001). Neurons derived from radial glial cells establish radial units in neocortex. Nature *409*, 714–720.

Orosco, L.A., Ross, A.P., Cates, S.L., Scott, S.E., Wu, D., Sohn, J., Pleasure, D., Pleasure, S.J., Adamopoulos, I.E., and Zarbalis, K.S. (2014). Loss of Wdfy3 in mice alters cerebral cortical neurogenesis reflecting aspects of the autism pathology. Nat. Commun. *5*, 4692.

Oshidari, R., Huang, R., Medghalchi, M., Tse, E.Y.W., Ashgriz, N., Lee, H.O., Wyatt, H., and Mekhail, K. (2020). DNA repair by Rad52 liquid droplets. Nat. Commun. *11*, 695.

Petroski, M.D., and Deshaies, R.J. (2005). Mechanism of Lysine 48-Linked Ubiquitin-Chain Synthesis by the Cullin-RING Ubiquitin-Ligase Complex SCF-Cdc34. Cell *123*, 1107–1120.

Pickart, C.M. (2001). Mechanisms Underlying Ubiquitination. Annu. Rev. Biochem. *70*, 503–533.

Popovitchenko, T., Park, Y., Page, N.F., Luo, X., Krsnik, Z., Liu, Y., Salamon, I., Stephenson, J.D., Kraushar, M.L., Volk, N.L., et al. (2020). Translational derepression of Elavl4 isoforms at their alternative 5' UTRs determines neuronal development. Nat. Commun. *11*, 1674.

Protter, D.S.W., and Parker, R. (2016). Principles and Properties of Stress Granules. Trends Cell Biol. *26*, 668–679.

Rao, B.S., and Parker, R. (2017). Numerous interactions act redundantly to assemble a tunable size of P bodies in Saccharomyces cerevisiae. Proc. Natl. Acad. Sci. *114*, E9569–E9578.

Rodrigues, D.C., Harvey, E.M., Suraj, R., Erickson, S.L., Mohammad, L., Ren, M., Liu, H., He, G., Kaplan, D.R., Ellis, J., et al. (2020). Methylglyoxal couples metabolic and translational control of Notch signalling in mammalian neural stem cells. Nat. Commun. *11*, 2018.

Sanders, D.W., Kedersha, N., Lee, D.S.W., Strom, A.R., Drake, V., Riback, J.A., Bracha, D., Eeftens, J.M., Iwanicki, A., Wang, A., et al. (2020). Competing Protein-RNA Interaction Networks Control Multiphase Intracellular Organization. Cell *181*, 306-324.e28.

Schneider-Poetsch, T., Ju, J., Eyler, D.E., Dang, Y., Bhat, S., Merrick, W.C., Green, R., Shen, B., and Liu, J.O. (2010). Inhibition of Eukaryotic Translation Elongation by Cycloheximide and Lactimidomycin. Nat. Chem. Biol. *6*, 209–217.

Schwamborn, J.C., Berezikov, E., and Knoblich, J.A. (2009). The TRIM-NHL Protein TRIM32 Activates MicroRNAs and Prevents Self-Renewal in Mouse Neural Progenitors. Cell *136*, 913–925.

Taal, K., Tuvikene, J., Rullinkov, G., Piirsoo, M., Sepp, M., Neuman, T., Tamme, R., and Timmusk, T. (2019). Neuralized family member NEURL1 is a ubiquitin ligase for the cGMP-specific phosphodiesterase 9A. Sci. Rep. *9*, 1–12.

Tai, H.-C., and Schuman, E.M. (2008). Ubiquitin, the proteasome and protein degradation in neuronal function and dysfunction. Nat. Rev. Neurosci. *9*, 826–838.

Teixeira, D., Sheth, U., Valencia-Sanchez, M.A., Brengues, M., and Parker, R. (2005). Processing bodies require RNA for assembly and contain nontranslating mRNAs. RNA N. Y. N *11*, 371–382.

Tenekeci, U., Poppe, M., Beuerlein, K., Buro, C., Müller, H., Weiser, H., Kettner-Buhrow, D., Porada, K., Newel, D., Xu, M., et al. (2016). K63-Ubiquitylation and TRAF6 Pathways Regulate Mammalian P-Body Formation and mRNA Decapping. Mol. Cell *62*, 943–957.

Tse, W.K.F., Jiang, Y.-J., and Wong, C.K.C. (2013). Zebrafish transforming growth factor-β-stimulated clone 22 domain 3 (TSC22D3) plays critical roles in Bmp-dependent dorsoventral

patterning via two deubiquitylating enzymes Usp15 and Otud4. Biochim. Biophys. Acta *1830*, 4584–4593.

Tuoc, T.C., and Stoykova, A. (2008). Trim11 modulates the function of neurogenic transcription factor Pax6 through ubiquitin–proteosome system. Genes Dev. *22*, 1972–1986.

Ukmar-Godec, T., Hutten, S., Grieshop, M.P., Rezaei-Ghaleh, N., Cima-Omori, M.-S., Biernat, J., Mandelkow, E., Söding, J., Dormann, D., and Zweckstetter, M. (2019). Lysine/RNA-interactions drive and regulate biomolecular condensation. Nat. Commun. *10*, 2909.

Van Treeck, B., and Parker, R. (2018). Emerging Roles for Intermolecular RNA-RNA Interactions in RNP Assemblies. Cell *174*, 791–802.

Vessey, J.P., Amadei, G., Burns, S.E., Kiebler, M.A., Kaplan, D.R., and Miller, F.D. (2012). An Asymmetrically Localized Staufen2-Dependent RNA Complex Regulates Maintenance of Mammalian Neural Stem Cells. Cell Stem Cell *11*, 517–528.

Wang, C., Schmich, F., Srivatsa, S., Weidner, J., Beerenwinkel, N., and Spang, A. (2018). Context-dependent deposition and regulation of mRNAs in P-bodies. ELife *7*.

Wheeler, J.R., Matheny, T., Jain, S., Abrisch, R., and Parker, R. (2016). Distinct stages in stress granule assembly and disassembly. ELife *5*, e18413.

Wilczynska, A., Aigueperse, C., Kress, M., Dautry, F., and Weil, D. (2005). The translational regulator CPEB1 provides a link between dcp1 bodies and stress granules. J. Cell Sci. *118*, 981–992.

Wu, J., Zhao, Z., Kumar, A., Lipinski, M.M., Loane, D.J., Stoica, B.A., and Faden, A.I. (2016). Endoplasmic Reticulum Stress and Disrupted Neurogenesis in the Brain Are Associated with Cognitive Impairment and Depressive-Like Behavior after Spinal Cord Injury. J. Neurotrauma *33*, 1919–1935.

Xie, Z., Hur, S.K., Zhao, L., Abrams, C.S., and Bankaitis, V.A. (2018). A Golgi Lipid Signaling Pathway Controls Apical Golgi Distribution and Cell Polarity during Neurogenesis. Dev. Cell *44*, 725-740.e4.

Xu, G., and Jaffrey, S.R. (2011). The new landscape of protein ubiquitination. Nat. Biotechnol. *29*, 1098–1100.

Yan, X., Hoek, T.A., Vale, R.D., and Tanenbaum, M.E. (2016). Dynamics of Translation of Single mRNA Molecules In Vivo. Cell *165*, 976–989.

Yang, G., Smibert, C.A., Kaplan, D.R., and Miller, F.D. (2014). An eIF4E1/4E-T Complex Determines the Genesis of Neurons from Precursors by Translationally Repressing a Proneurogenic Transcription Program. Neuron *84*, 723–739.

Yasuda, S., Tsuchiya, H., Kaiho, A., Guo, Q., Ikeuchi, K., Endo, A., Arai, N., Ohtake, F., Murata, S., Inada, T., et al. (2020). Stress- and ubiquitylation-dependent phase separation of the proteasome. Nature *578*, 296–300.

Youn, J.-Y., Dunham, W.H., Hong, S.J., Knight, J.D.R., Bashkurov, M., Chen, G.I., Bagci, H., Rathod, B., MacLeod, G., Eng, S.W.M., et al. (2018). High-Density Proximity Mapping Reveals the Subcellular Organization of mRNA-Associated Granules and Bodies. Mol. Cell *69*, 517-532.e11.

Zahr, S.K., Yang, G., Kazan, H., Borrett, M.J., Yuzwa, S.A., Voronova, A., Kaplan, D.R., and Miller, F.D. (2018). A Translational Repression Complex in Developing Mammalian Neural Stem Cells that Regulates Neuronal Specification. Neuron *97*, 520-537.e6.

Zhang, M., Chen, D., Xia, J., Han, W., Cui, X., Neuenkirchen, N., Hermes, G., Sestan, N., and Lin, H. (2017). Post-transcriptional regulation of mouse neurogenesis by Pumilio proteins. Genes Dev. *31*, 1354–1369.

Zhao, Y., Majid, M.C., Soll, J.M., Brickner, J.R., Dango, S., and Mosammaparast, N. (2015). Noncanonical regulation of alkylation damage resistance by the OTUD4 deubiquitinase. EMBO J. *34*, 1687–1703.